8-2017

Detection and Quantification of Biological and Physiochemical Parameters in Porous Media

Biting Li
Clemson University, 544874114@qq.com

DETECTION AND QUANTIFICATION OF BIOLOGICAL AND PHYSIOCHEMICAL PARAMETERS IN POROUS MEDIA

A Thesis
Presented to
the Graduate School of
Clemson University

In Partial Fulfillment
of the Requirements for the Degree
Master of Science
Biosystems Engineering

---

by
Biting Li
August 2017

Accepted by:
Dr. Christophe Darnault, Committee Chair
Dr. Brian Powell
Dr. Yi Zheng
Dr. William Bridges

ABSTRACT

Three studies were conducted in this thesis, and all were related to measurement of biological and physiochemical parameters in porous media. The first study focused on the detection of biological parameter, and investigated the effects of cerium oxide nanoparticles on soil enzyme activity. Different concentrations of soil-NP mixture were applied, and exposure time length in addition to the harvest events were considered during the experiments. The second study focused on the quantification of physical parameter, and revealed water saturation percentage profiles during infiltration process along the preferential flow fingers. Two microbial exudates, catechol and riboflavin, with varying concentrations were applied to the flow experiments. Light transmission method was utilized to acquire information of light intensity, which was later converted to water saturation percentage. The third study focused on the measurement of physiochemical parameters, and evaluated the pH and dissolved oxygen concentration gradients in 2D tank sand system. Optical image technique was used to obtain data, and emitted fluorescence from the sensor foils were captured by the camera.

TABLE OF CONTENTS

Page

Table of Contents (Continued)

Page

LIST OF TABLES

LIST OF FIGURES

List of Figures (Continued)

Figure Page

List of Figures (Continued)

Figure Page

CHAPTER ONE

INTRODUCTION

Three independent studies were described in this thesis, and all three studies took place in porous media. Different aspects of biological and physiochemical parameters were measured and examined. More details are shown in later chapters.

The objective of the first study was to primarily determine whether CeO_2 NPs would affect soil quality and fertility by changing soil enzyme activities. Engineered nanoparticles (NPs) released in the soil, water, and air can return to the environment through the agronomic land application of biosolids, and their potential effect on agricultural ecosystems is most concerning. Soil enzyme activity, often treated as an indicator of soil quality and soil biota, is also useful in determining the sustainability of agricultural ecosystems, particularly the soil physico-chemical and microbiological processes. The concentration and exposure time-dependent potential toxicity of CeO_2 NPs on soil microorganisms was examined by testing the activity of three enzymes--urease, phosphatase and ß-glucosidase—in a soil-grass microcosm system, and estimated through specific enzyme assays. NPs were applied at different concentrations at 0, 100, 500 and 1000mg/kg soil mixtures in separated pots in which organic hard red wheat (*Triticum aestivum*) was grown. The effect of exposure time of NPs on soil enzyme activity was also examined through different harvest time events, by cutting the wheatgrasss in cut group at week two (cut 1), thirteen (cut 2) and twenty two (cut 3) and analyzing the soil enzyme activities, which were then compared with those in non-cut groups.

The primary objective of the second study entailed an investigation of how different microbial exudates with varying concentrations alter the infiltration process in an unsaturated sand system and the distribution of the soil moisture content. Specifically, the microbial exudates catechol and riboflavin were examined to determine any influence of flow in porous media. In the hydrological cycle, the infiltration process is a critical component in the distribution of water into the soil and in groundwater system which provides millions of individuals worldwide with potable water. As a major flow pattern, the preferential flow that interacts with microbial and plant activity has been analyzed in heterogeneous media. Although the relationship between the plant root exudates and water transport in soil has been the subject of extensive study, only a few cases of microbial exudates are available in the literature. Here the authors investigated the influence of two artificial microbial exudates–catechol and riboflavin–on preferential flow process, and to specifically show the various concentrations acting upon them. The experiments were conducted in a two-dimensional initially dry tank that was filled with quartz sand with the contact angle and surface tension measured to obtain the interfacial forces. The light transmission method (LTM) was used to capture light intensity, which was then converted into a percentage of vertical and horizontal soil water saturation profiles.

The main objective of third study was to evaluate the performance of pH and O_2 sensor foils in porous media with simulated scenarios. Understanding the spatial and temporal distribution of physical and chemical parameters (e.g. pH, O_2) is imperative to characterize the behavior of contaminants in a natural environment. As a non-invasive

method, the optical imaging technique utilizes optical sensor foils and a digital camera to acquire data. Calibration experiments measured pH value in the range from 3 to 7, and dissolved oxygen concentration from 0 mg/L to 20.74 mg/L. Application tests of sensor foils involved zero valent iron (ZVI) and sulfuric acid drainage solution in order to obtain gradients of parameter changes.

CHAPTER TWO

INFLUENCE OF CERIUM OXIDE NANOPARTICLES ON THE SOIL ENZYME ACTIVITIES IN A SOIL-GRASS MICROCOSM SYSTEM

1. Introduction

Engineered nanoparticles have been developed in large quantities for use in a wide range of industrial applications (Casals et al., 2008; Keller et al., 2013; Roco, 2011). This significant and widespread use of engineered nanoparticles following accidental releases or from end of life cycle disposal has made their introduction into the environment inevitable (Gottschalk and Nowack, 2011). Nanoparticles in sizes ranging from 1 to 100 nm and with unique physico-chemical properties are not only be valuable materials to science and industry, but also hazardous materials to the environment and organisms (Klaine et al., 2008). Therefore, exploring the potential impacts of engineered nanoparticles in the environment is critical to assess the toxicity risk to human health and ecosystems. The potential effect of engineered nanoparticles on agricultural ecosystems, particularly on their soil physico-chemical and biological processes is most concerning. Nanoparticles come in contact with soil and plants through deposition from the atmosphere, transportation through bodies of water bodies, and through the application of nanofertilizers and biosolids in wastewater sludge (Gardea-Torresdey et al., 2014; Gogos

et al., 2012; Keller et al., 2013; Suppan, 2013). As a cheaper nutrient and organic matter alternative to fertilizers, biosolids are widely used in agriculture (Antolín et al., 2010). However, those biosolids may contain high concentrations of engineered nanoparticles based on types (Gottschalk et al., 2013; Keller and Lazareva, 2014).

Of the many engineered nanoparticles available, cerium oxide nanoparticles (CeO_2 NPs) are of particular concern in that the level of production and use of CeO_2 NPs are immense (Piccinno et al., 2012). CeO_2 NPs, are normally used as additives to catalyze diesel fuel engine systems to reduce emissions, as agents to polish materials such as glass, and as materials for UV light adsorption (Cassee et al., 2011; Dahle and Arai, 2015; EPA, 2009; HEI, 2001).

There are several pathways by which CeO_2 NPs may find their way into the environment. For example, cerium oxides from abandoned engines and polished materials drift into the environment and are transported into water bodies and soil systems. CeO_2 NPs are also present in both the effluents and biosolids of wastewater treatment plants (Barton et al., 2015; Blaser et al., 2008; Limbach et al., 2008). The potential amounts of CeO_2 NPs ending up in the soil, water, air, and landfill have been assessed at 1,400, 300, 100, and 8,200 metric tons/year, respectively (Keller et al., 2013).

Therefore, it is critical to undertake research to elucidate the effect of engineered nanoparticles in the soil-water environment, particularly in terms of the possible ecotoxicological effects (Handy et al., 2008a,b; Unrine et al., 2008), as they may be released for the first time in the soil, water and air, or as they may return to the environment for a second time through the agronomic land application of biosolids.

Many studies undertaken to investigate the toxicological effects of nanoparticles have focused on aquatic and terrestrial microorganisms (Blaise et al., 2008; Jemec et al., 2008; Lovern et al., 2007; Lovern and Klaper, 2006; Roh et al., 2010; Velzeboer et al., 2008; Wang et al., 2009), and microbes (Antisari et al., 2013; Bae et al., 2010; Bandyopadhyay et al., 2012; Fang et al., 2010; Frenk et al., 2013; Gajjar et al., 2009; Lee et al., 2009; Pelletier et al., 2010). However, few studies have investigated the potential influence of engineering nanoparticles on soil enzyme activities (e.g. Jośko et al., 2014; Tong et al., 2007). Indeed, the alterations of soil enzymes activities may affect soil biological systems which may have important ecological and economical outcomes.

The evaluation of microbial activity as an indicator of soil quality to assess environmental changes is more rapid and sensitive than monitoring soil physico-chemical properties. The elements and phenomena that affect soil microbial activity also govern soil enzyme activities that are integral to soil biology, and nutrient cycling within plants (Sinsabaugh et al., 1993). As a consequence, soil enzyme activity is one indicator of soil quality and soil biota, and therefore larger indicator of the sustainability of agricultural ecosystems, particularly the soil physico-chemical and microbiological processes (Aon and Colaneri, 2001). Soil enzyme activity is a sensitive indicator of changes on soil quality and fertility, particularly for nutrient availability, as well as soil biota that are induced by and through the environment (Chen et al., 2003). Water is not only a limiting factor in agricultural ecosystems. Indeed, the availability of essential nutrients of nitrogen and phosphorus are important for the sustainable growth and development of agricultural ecosystems.

Very limited data is available on the effect of nanoparticles on soil enzyme activities, and the data that is available indicates conflicting activity responses when different enzymes were exposed to nanoparticles. Specifically, ZnO, Cr_2O_3, CuO and Ni NPs (10, 100 and 1000 μg g^{-1} soil) exhibited inhibiting and promoting effects on the activities of acid and alkaline phosphatases, dehydrogenase, and urease, as a function of soil type, contact time, and NP size (Jośko et al., 2014). Also Ag NPs (1-100 μg g^{-1} soil) inhibited the activities of phosphomonoesterase, arylsulfatase, β-D-glucosidase, and leucine-aminopeptidase (Peyrot et al., 2014). Ag NPs (1-1,000 μg g^{-1} soil) may inhibit the activities of urease, acid phosphatase, arylsulfatase, β-glucosidase (Shin et al., 2012). Although Ag NPs (0.32 μg g^{-1} soil) did not affect the activities of β-glucosidase, β-cellobiohydrolase, acid phosphatase, chitinase, and xylosidase, a limited inhibition was observed on the activity of the leucine-aminopeptidase (Hänsch and Emmerling, 2010). Zero valent iron nanoparticles (10,000 μg g^{-1} soil) promoted the activity of dehydrogenase, while the activity of fluorescein diacetate hydrolase was not hindered (Cullen et al., 2011). In addition, Zn and ZnO NPs (2,000 μg g^{-1} soil) was observed to inhibit the activities of acid phosphatase, β-glucosidase, and dehydrogenase (Kim et al., 2011). Multiwall carbon nanotubes (5,000 μg g^{-1} soil) exhibited a negative effect on the activities of β-glucosidase, β-N-acetylglucosaminidase, acid phosphatase, cellobiohydrolase, and xylosidase (Chung et al., 2011). However, the single walled carbon nanotubes (1-1,000 μg g^{-1} soil) decreased the activities of b-1,4-glucosidase, b-1,4-xylosidase, b-1,4-N-acetylglucosaminidase, cellobiohydrolase, while the activities of the L-leucine aminopeptidase was increased (Jin et al., 2013). Although fullerene

nanoparticles were observed to limit the inhibition of the activities of urease, acid phosphatase, β-glucosidase, and dehydrogenase (Tong et al., 2007). TiO_2 and ZnO NPs significantly enhanced the activities of catalase, protease and peroxidase, while no effects of the activity of urease were increased (Du et al., 2011).

Unfortunately, little is known about ecotoxicological effects of CeO_2 on the critical biogeochemical cycles, particularly on soil enzyme activities linked to the C, N and P cycles. Urease, phosphatase and β-glucosidase are microbe-produced enzymes of primary importance for their role in the C, N and P cycles in various soil ecosystems. Urease, which is an indicator of soil quality for nitrogen cycling, acts on organic matter containing nitrogen, mostly urea, and produces inorganic nitrogen ammonia (NH_3), which then is transformed to ammonium (NH_4) and available for the uptake in plants (Bandick and Dick, 1999; Zimmer, 2000). This microbial-secreted urease is very resistant to environmental breakdown in the soil (Zantua and Bremner, 1977). Phosphatase, which indicates phosphorous cycling in the soil-plant system, hydrolyzes organically-formed phosphorus into plant-available phosphate (Henneberry et al., 1979). ß-glucosidase, which is an excellent indicator of decomposition of organic matter in the soil, produces simple sugars and smaller organic structures to provide energy for soil microbes and enable further microbial enzyme activity (Bandick and Dick, 1999).

Introduction of CeO_2 NPs to soil ecosystems may occur repeatedly as waste water, biosolids, and/or fertilizers are applied to land surfaces. Significant environmental doses of CeO_2 NPs may accumulate in soils as a result of these repeated applications because of agricultural practices. Consequently, these environmental conditions create a

realistic exposition of soil microorganisms to CeO_2 NPs. Our research focuses on how CeO_2 NPs impact soil quality and the aging effects of nanoparticles. We work with CeO_2 NPs that may be introduced to agricultural soils through the land application of biosolids, waste water, in phosphate fertilizers, or dispersed in diesel engine exhaust. The main objective of this research was to investigate the effect of CeO_2 NPs on biochemical soil quality indicators--soil enzyme activities--in order to evaluate their toxicity to soil ecosystems. To test the potential toxicological effects of CeO_2 NPs on the soil biochemical dynamics, we performed a study that involved microcosms that were prepared using agricultural soil from Illinois and organic soil and planted with wheatgrass. An accelerated cropping management and harvesting system was employed under a sodium grow light to simulate normal growth over time and regrowth of plants following harvest—wheatgrass cutting—events, under different CeO_2 concentrations (0, 100, 500 and 1000 mg kg^{-1} soil). Three harvests over 22 weeks were performed for the normal growth (also known as non-cut group). Similarly, over the same period, three cuts and three harvests of the plants were also performed to simulate plants regrowth. At the time of each harvest, soil enzymes activities were examined as a function of various dose treatments of CeO_2 NPs, enzyme types, contact time and cut type. Urease, phosphatase and β-glucosidase were the three enzymes selected to examine in this study because of the critical role these soil enzymes play in biogeochemical cycles, particularly linked to the C, N and P cycles. Each enzyme had a specific assay to detect its activity.

2. Material & Methods

2.1 Soil preparation

The soil was composed of a mixture of a Gilford and an organic soil. The soil mixture was prepared by adding 250 g of Gilford soil and 125 g of organic soil in a 2:1 ratio. The physico-chemical characteristics of the Gilford soil, which was a sandy loam soil collected from Kankakee County, Illinois, were established by the Utah State University Analytical Laboratories (USUAL). It had 84.40% sand, 7.70% silt and 7.90 clay. Soil pH was 5.20; electrical conductivity was 0.68 dS m^{-1}; total organic matter content ranged from 3.30% (Walkey-Black method) to 4.20% (loss on ignition method); total nitrogen was 0.19%; and soil carbon was 2.91% for total carbon (TC) and 2.91% for total organic carbon (TOC). The organic soil (Harvest, Waltham, MA) was composed of organic matter and organic fertilizer, which provided soil mixture with nutrients and good porosity for air and water movement. It had 0.1% of total nitrogen, 0.05% of available phosphate in the form of P_2O_5, and 0.05% of soluble potash as K_2O. For each pot, 375 g of dry soil mixture was measured on the NewClassic MS3002S Balance (Mettler Toledo, Columbus, OH) and mixed in High-Density Polyethylene (HDPE) wide mouth bottles (VWR International, Radnor, PA) by shaking. The physico-chemical characteristics of the soil mixture were analyzed by the Agricultural Service Laboratory at Clemson University (Table 2.1). Among the measurements tested to evaluate the initial conditions of the soil mixture, analyses showed a pH value of 5.7, an organic matter content of 5.40 %, and a cerium concentration of 0.148 ppm (Table 2.1).

2.2 Nanoparticle suspension preparation

Cerium (IV) oxide with a nanopowder size smaller than 25 nm was obtained from Sigma-Aldrich, St. Louis, MO. A MX5 Microbalance (Mettler Toledo, Columbus, OH) was used to prepare the specific masses of nanoparticles under a 2' XPert Nano Enclosure (Labconco, Kansas City, MO), which filtered nanoparticle powders and provided protection during the operation processes. Four concentrations of CeO_2 nanoparticle were applied to the soil, which were 0 mg/kg soil, 100 mg/kg soil, 500 mg/kg soil and 1000 mg/kg soil. The quantities of CeO_2 prepared for each concentration were 0 g, 0.675 g, 3.375 g, and 6.75 g, respectively. The weighted CeO_2 nanopowder were then dispersed using the Sonicator 4000 (Misonix Inc, Farmingdale, NY) with an operating frequency of 20 kHz and power rating of 600 Watts for ten minutes in 100 mL of 18.2 MΩ•cm of ultrapure deionized (DI) water (Millipore Corporation, Billerica, MA). The nanoparticle solution was further diluted to one liter of volume using ultrapure DI water. Nanoparticle suspensions were kept dispersing in the Bransonic® CPXH Ultrasonic Baths with a frequency of 40 kHz and high power control (Emerson Electric, St. Louis, MO) before they were added to the soil mixtures.

2.3 Soil-Nanoparticle mixture preparation

The 1L of mixed nanoparticle suspension for every concentration was divided into 18 portions, and each soil mixture (375 g) was watered with 55.6 ml of the suspension and then mixed in a seed pot with a diameter of 4.5 inch (Clovers Garden, North Riverside, IL) with a small garden shovel. The complete soil-nanoparticle mixtures were reloaded into the pots according to the corresponding concentrations. Seventy two pots with separate trays were prepared based on four concentrations of nanoparticles and

six sets of groups. The replicates contained three cut groups, two non-cut groups and one additional backup cut group to ensure that the live plant system in the pots were present at time of harvest, which were all done in triplicates.

2.4 Germination of wheatgrass

Organic Hard Red Wheat (*Triticum aestivum*) was selected as the crop for growth in the soil-nanoparticle mixtures to establish a soil-plant microcosm system. Fifteen grams of Organic Hard Red Wheat with a purity of 99% (Todd's Seeds, Novi, MI) were weighted for each pot and disinfected using NaClO solution with 5% of available Cl (Fisher Scientific, Waltham, MA). The seeds were first washed in the sodium hypochlorite solution for 30 seconds and were rinsed by ultrapure DI water for three times (Kiemnec et al., 2003). The disinfected seeds were then soaked with a layer of water in containers for 12 hours, covered with a wet paper towel after draining and left to sit for another 12 hours. The disinfection and soaking process helped germination and the seeds were ready to grow in the soil after this step.

2.5 Seeding

The germinated seeds were spread evenly on the soil surface in the pots with the top 1 cm of soil temporally removed. The seeds were again loosely covered with the previously removed layer of soil, and watered.

2.6 Growing of plants

Seventy two pots were randomly placed on a table in trays under a Yield Master 8in Air Cooled Reflector (Sunlight Supply, Vancouver, WA) having a Hortilux 1000 Watt High Pressure Sodium Bulb (Eye Lighting, Mentor, Ohio) installed. The sodium

bulb was specifically designed to promote plant growth by giving sufficient spectral energy, and was connected to a Galaxy Grow Amp 1000 Watt and 600/750/1000/Turbo charge electronic ballast (Sunlight Supply, Vancouver, WA). The whole lighting unit was hooked to a Sun Stand (Sunlight Supply, Vancouver, WA) with an adjustable height from 52in to 88in. The day light length was adjusted to be about 12 hours per day, and the plants were watered every two to three days. After every harvest, the regrowth of wheatgrass required more nutrients. To be consistent, the non-cut groups also got access to them. The nutrient solutions were prepared by adding one packet (12g) of soluble fertilizers (The Scotts Miracle-Gro Company, Marysville, OH), containing 3.5% of ammoniacal nitrogen, 20.5% of urea nitrogen, 8% of available phosphate (P_2O_5) and 16% of soluble potash (K_2O), to two gallons of ultrapure DI water, and were applied to plants via watering.

2.7 Harvest

Counting from the first day of seeding, the whole growing period was five months. Plants were harvested at two week, thirteen week, and twenty-two week intervals after the seeding event, respectively. After each harvest, all sets of pots for the cut groups were mowed and the sets for the non-cut groups continued to grow until the next harvest assigned. The sets of targeted pots for each harvest were then destroyed for soil and enzyme analyses. During the first harvest, one set of cut group for each concentration was destroyed, and all cut groups were mowed. For the second harvest, one set of cut group in addition to a set of non-cut group were destroyed, and all cut groups were mowed again.

For the third harvest, one set of cut group and the last set of non-cut group were destroyed.

2.8 Soil sampling

Soil was separated from the massive roots as cleanly as possible by avoiding large chunks of wood chips and roots. Twelve grams (2g each) of wet soil samples from different locations in the pot were collected, and three portions of 2g wet soil were used to calculate the dry soil mass after oven-drying to determine soil enzyme activity. The other three portions of the 2g of wet soil were blended with 50 mM, pH 5 acetate buffer, made from sodium acetate trihydrate (≥ 99%, Sigma-Aldrich, St. Louis, MO), as soil suspensions in triplicates for further enzyme analysis.

2.9 Enzyme activity analysis

Three enzymes were tested: urease (EC 3.5.1.5), phosphatase (EC 3.1.3.2) and β-glucosidase (EC 3.2.1.21), with urea (Sigma-Aldrich, St. Louis, MO) used as the substrate for the urease protocol (Allison, 2001a). The 50 mM acetate buffer was made from sodium acetate trihydrate (≥ 99%, Sigma-Aldrich, St. Louis, MO), glacial acetic acid (≥ 99%, Sigma-Aldrich, St. Louis, MO) and ultrapure DI water. The soil suspensions were mixed with both the substrates and the buffer for sample groups and suspension controls, respectively, and done in triplicate. Three substrate controls were also conducted without soil suspensions. After incubation for two hours at room temperature, sodium salicylate (≥ 99.5%, Sigma-Aldrich, St. Louis, MO), sodium nitroprusside (Sigma-Aldrich, St. Louis, MO) and BDH ACS Grade sodium hydroxide (VWR International, Radnor, PA) were mixed with ultrapure DI water. This solution was then

added to the soil supernatant, which was obtained by centrifugation at a speed of 10,000 rpm for one minute using Centrifuge 5810R (Eppendorf, Hamburg, Germany). Sodium dichloroisocyanurate (96%, Sigma-Aldrich, St. Louis, MO) was finally added to halt the reaction and to develop color. An Epoch 2 Microplate Reader (BioTek, Winooski, VT) was then used to read the optical density. The urease activity was calculated as:

Activity ($\mu mol\ NH_4\ h^{-1}\ g^{-1}$) =

Final OD / [(EC/μmol/ml)/(1.5ml/assay)(incubation time, h)(g dry soil used to make sample suspension / ml sample suspension) (0.75 ml sample suspension)]

where OD was the optical density read from the Microplate Reader, EC was the slope value obtained from the standard curve.

The final OD value was calculated by subtracting the OD values of sample controls and substrate controls from sample assays. The EC value for urease was 0.9751 ml/μmol. The substrates used for the phosphatase and β-glucosidase protocols (Allison, 2001b), were p- Nitrophenyl phosphate (Sigma-Aldrich, St. Louis, MO) and 4-Nitrophenyl β-D-glucopyranoside (≥ 98%, Sigma-Aldrich, St. Louis, MO), respectively.

A similar method of preparation was used to incubate the phosphatase samples for 45 min and β-glucosidase samples for 1 h. The reactions of the supernatants were then terminated by adding 1N of NaOH. After adding ultrapure DI water to dilute, the Microplate Reader was used to read the developed colors at 410 nm. The phosphatase and β-glucosidase activity were both calculated as:

Activity ($\mu mol\ h^{-1}\ gDOM^{-1}$) =

Final OD / [(EC/μmol/ml)/(1.5ml/assay)(incubation time, h) (gDOM / ml

sample suspension) (0.75 ml sample suspension)]

where gDOM was the oven dried mass from 2g of wet soil sample.

The final OD value was calculated by subtracting the OD values of the sample controls and the substrate controls from the sample assays. The EC value for phosphatase and β-glucosidase was 2.2369 ml/μmol.

2.10 Statistical analysis

General Linear Models were developed that related the means of the three enzyme concentrations to the effects of the experimental factors (concentration, treatment) at the different harvests. ANOVA was used to test the statistical significance of the experimental factors. When factors were determined to be statistically significant, Tukey's Honestly Significant Difference (HSD) was used to make specific comparisons among the factor level means. Results are reported as the enzyme means and associated standard errors.

ANOVA assumptions of normal distribution and homogeneity of variance were assessed and found to be satisfied. Statistical significance was set at an alpha value of 0.05. Microsoft Excel 2010 and JMP Pro 12 were used for all calculations.

Inhibition and promotion percentages were calculated in Microsoft Excel 2010 using the equation shown below:

$$\% \text{ inhibition/promotion} = \frac{C_t - C_0}{C_0} \times 100\%$$

where, C_t is the enzyme activity at different treatments with CeO_2 NP present, and C_0 is the enzyme activity at 0 mg/kg CeO_2 NP concentration within each cut. The calculated

negative values were treated as inhibition effect, while the calculated positive values were considered as promotion effect.

3. Results

Three types of soil enzyme activities were measured and analyzed after each of the three harvest events as non-cut and cut groups. A comparison of the first harvest and the control group without CeO_2 NPs indicated a significant decrease in the activities for urease and β-glucosidase, and an overall increase in phosphatase activity. The results also indicated a different influence of the CeO_2 NPs on the respective soil enzyme activities, depending on enzyme type, NP dose, contact time, and plant harvest event.

3.1 Effect of concentration of CeO_2 NPs on enzyme activities

3.1.1 Urease activity

An increased concentration of CeO_2 NPs resulted in a corresponding decrease in the urease activity for each harvest of the non-cut group (Figure 2.1a). For the cut group, a decrease in activity was also observed for the first and second harvest events, with no such obvious trend observed for the third harvest (Figure 2.1b). The negative effects from CeO_2 NPs on urease activity are shown in Figures 2.2a and 2.2b. The increasing trend for each harvest event indicated a more negative influence on urease enzyme activity at higher concentrations. Specifically, for the non-cut 1 and cut 1 groups, the inhibition effect increased from a -5.07% at a 100 mg/kg concentration to -13.2% at a 500 mg/kg concentration to -19.91% at a 1000 mg/kg concentration compared to the treatment without CeO_2 NPs. An inconsistency of positive values of 15.18% and 6.88% at

concentrations of 500 mg/kg and 1000 mg/kg, respectively, was observed for the cut 3 group.

Significant differences were observed in the urease non-cut group samples, however, between 0 and 500 mg/kg, 0 and 1000 mg/kg, and 100 and 1000 mg/kg concentrations at the first harvest. At the second and third harvest, the significant differences between 100, 500 and 1000 mg/kg concentrations were observed to diminish (Figure 2.1a), as was a clear difference between pots with nanoparticles and pots without nanoparticles. As time increased, the low concentrations (100 and 500 mg/kg) with no detectable differences did have an effect on the enzyme activity, compared to 0 mg/kg concentration. A possible threshold affect was observed in the second and third harvests of the non-cut group, with the presence or absence of nanoparticles falling into two distinct categories. Although the differences between the cut and non-cut groups for urease were identical for the first harvest, no significant difference was observed between all concentrations for the second and third harvests (Figure 2.1b). These trends indicated a significant decrease in the difference between urease concentrations with a corresponding increasing in time regarding urease activity.

3.1.2 Phosphatase activity

For both the non-cut and cut groups, except for the second and third harvests where no large difference between concentrations of 0, 100 and 500 mg/kg (Figure 2.1c, 2.1d) were observed, the phosphatase activity increased for each harvest event with a corresponding increase in concentration. Using this positive trend observed for phosphatase activities, promotion percentages, as shown in Figure 2.2c and 2.2d, were

calculated based on the concentration of 0 mg/kg at each concentration. The non-cut and cut 1 groups exhibited the greatest effect on promotion, with an increase from 97.46% to 131.37% to 181.45% at 100, 500 and 1000 mg/kg concentrations, respectively, compared to the 0 mg/kg concentration.

Significant differences were observed within the phosphatase non-cut group between 0 and 100 mg/kg, 0 and 500 mg/kg, 0 and 1000 mg/kg, 100 and 1000 mg/kg concentrations at the first harvest. At the second harvest, significant differences were observed between 0 and 100 mg/kg, 0 and 500 mg/kg, 0 and 1000 mg/kg, 100 and 1000 mg/kg, and 500 and 1000 mg/kg concentrations. At the third harvest, these differences were reduced to only a range between 0 and 500 mg/kg, and 0 and 1000 mg/kg (Figure 2.1c). A possible proportional effect - CeO_2 NPs dose dependent relationship - was observed in all three harvest events. Among the cut group for phosphatase, significant differences were identical for the non-cut group at the first harvest. Although no significant difference in NP presence was observed between the concentrations of 0, 100 and 500 mg/kg at the time of second and third harvest, they differed significantly with the highest concentration of 1000 mg/kg (Figure 2.1d). The trends indicated that the significant difference between concentrations decreased with an increased timespan for phosphatase activity.

3.1.3 Beta glucosidase activity

For both the non-cut and cut groups, an increasing concentration caused decrease in the β-glucosidase activity was observed at the first and second harvest events, while it remained relatively constant at the third harvest event (Figure 2.1e, 2.1f). The negative

effects were observed for both non-cut and cut groups and at all concentration levels (Figure 2.2e, 2.2f). For the cut 2 group, the inhibition effect increased from -0.32% to -70.84% at the 100 mg/kg and 1000 mg/kg concentrations, while an inhibition percentage for the non-cut 2 group was between -16.89% to -50.22% at the 100 mg/kg and 1000 mg/kg concentrations.

Regarding the β-glucosidase non-cut group at the time of the first harvest, significant differences existed at concentrations between 0 and 500 mg/kg, 0 and 1000 mg/kg, 100 and 500 mg/kg, and 100 and 1000 mg/kg. At the time of the second harvest, significant differences existed at concentrations between 0 and 500 mg/kg, 0 and 1000 mg/kg, 100 and 1000 mg/kg, and 500 and 1000 mg/kg. At the time of the third harvest, no significant differences were observed at concentrations between 0, 100,500 and 1000 mg/kg (Figure 2.1e). Regarding the β-glucosidase cut group at the time of the first harvest, the significant differences were identical to that of the non-cut group. At the second harvest, however, significant differences were observed at concentrations between 0 and 500 mg/kg, 0 and 1000 mg/kg, 100 and 500 mg/kg, 100 and 1000 mg/kg, and 500 and 1000 mg/kg. At the time of the third harvest, no significant difference was observed between all four concentrations (Figure 2.1f). These trends indicated that the overall significant difference between concentrations decreased as the time increased for the β-glucosidase activity.

3.2 Effect of length of exposure time to CeO_2 NPs on enzyme activities

Variations were observed within each concentration between all harvesting events for both the cut and non-cut groups for all three enzyme types. As the time elapsed

towards the third harvest, a greater reduction in urease activity was observed. The urease activity for the non-cut group decreased from 0.0625 NH_4 h^{-1} g^{-1} to 0.0065 NH_4 h^{-1} g^{-1} at concentrations of 100 mg/kg, from 0.0571 NH_4 h^{-1} g^{-1} to 0.0048 NH_4 h^{-1} g^{-1} at concentrations of 500 mg/kg, and from 0.0527 NH_4 h^{-1} g^{-1} to 0.0038 NH_4 h^{-1} g^{-1} at concentrations of 1000 mg/kg. These trends indicated that a longer exposure time to CeO_2 NPs decreased the urease activity. A comparison of the non-cut and cut groups indicated at greater inhibition of urease activity in the cut group, especially at the second harvest event.

Phosphatase activities had higher values with an increase in time among the non-cut groups in all but the third harvest, where the activity subjected to 1000 mg/kg was lower than that of the second harvest. These trends indicated that a longer exposure time to CeO_2 NPs promoted phosphatase activity. A comparison of the non-cut and cut groups indicated less promotion of phosphatase activity in the cut groups in the presence of nanoparticles. At the 500 mg/kg concentration for non-cut groups, the phosphatase activities were 0.0417 μmol h^{-1} $g^{-1}$and 0.0454 μmol h^{-1} g^{-1} at the second and third harvests, and the activities for cut groups were reduced to 0.0295 μmol h^{-1} g^{-1} and 0.0342 μmol h^{-1} g^{-1}, correspondingly.

For the first and second harvest events among both non-cut and cut groups, a significant reduction of β-glucosidase activity was observed under each concentration. At the 100 mg/kg concentration, the β-glucosidase activity was reduced from 0.1941 μmol h^{-1} g^{-1} to 0.0142 μmol h^{-1} g^{-1} for the non-cut groups, and from 0.1941 μmol h^{-1} g^{-1} to 0.0240 μmol h^{-1} g^{-1} for the cut groups. At the third harvest, the activity for β-glucosidase was

slightly higher than that of the second harvest for non-cut group, while it was lower than that of the second harvest for cut group. The trends indicated that a longer exposure time to CeO_2 NPs inhibited the β-glucosidase activity at the first and second harvest events. This trend did not continue until time for the third harvest at which point the activity values were relatively constant for both non-cut and cut groups across the concentrations.

4. Discussion

As an important soil quality indicator, microbial activity and its related enzyme activity are possibly influenced by surrounding environment, due to the high sensitivity to changes in geochemical parameters and the accumulation of toxics either by intentional or unintentional applications. The relationship between nanoparticles and enzyme activities is hard to generalize, because it relies on specific properties of NPs: type and size, concentration applied, plant and enzyme type selected, and media composition (Dimkpa, 2014). In this study, enzyme types, different concentration treatments, contact time and cut type were examined. The soil enzyme activity was variously affected by the CeO_2 NPs, depending on the enzyme types. The experimental results showed that both urease and β-glucosidase activities were inhibited by CeO_2 NPs; and the higher concentration increased the inhibition except for urease in the third harvest event in that particular cut group. These results were consistent in that the highest percentage of inhibition percentage corresponded to the highest concentration of nanoparticles treated (Jośko et al., 2014). Although several enzyme activity data sets showed large standard deviations, these variations were thought to commonly exist in the

soil enzyme assays (Kim et al., 2011; Shin et al., 2012; Tong et al., 2007). It was determined, in one study undertaken to assess dehydrogenase, phosphatase and β-glucosidase, that all of these activities were reduced after the treatment with ZnO NPs (Kim et al., 2011). In an analysis of Xu et al. (2015) about the concentrations of CuO NPs and enzyme activities for both urease and phosphatase, a negative dose-response relationship was observed between each. It was determined that the decrease in enzyme activities from the CuO NP treatment was possibly due to the toxic effects from their heavy metal characteristics, which can inhibit enzyme activities by inactivating protein groups or blocking the binding sites on the enzymes (Dick et al., 1997; Kizilkaya and Bayrakli, 2005). It is also known that engineered nanoparticles of very small size with large surface-area-to-volume ratio are more reactive, unlike their bulk heavy metal counterparts, and thus have greater inhibition impacts on enzyme activity (Jośko et al., 2014). In this research, the authors presumed that the toxic properties of the engineered nanoparticles were responsible for the inhibition of soil enzyme activities. The possible mechanisms for such nanoparticle toxicity to soil organisms and plants are thought to be the generation of ROS, the disturbance of cell membranes, the disruption on electron transfer from the retaining of electrons, and the interaction with proteins within the cells (Pan and Xing, 2010). The results of a study involving the *Caenorhabditis elegans* (C. *elegans*) nematode suggested a positive correlation between the ROS accumulation, which caused oxidative damage to the C. *elegans* and exposure to CeO_2 NPs (Zhang et al., 2011). This evidence also indicated that the inhibition of both the urease and β-

glucosidase activity was possible due to the ROS accumulation, which would cause oxidative stress to the cells (Pan and Xing, 2010).

Nanoparticles, however, exhibited various influences on the enzyme activities, depending on the types of enzyme to which they were exposed. CeO_2 NPs were observed to inhibit the effects of urease and β-glucosidase activities, while a stimulation effect was recorded for phosphatase activity. For both the cut and non-cut groups, the promotion effect was greater at higher NP concentrations during the first harvest event, which was consistent with the inhibition results. An increased presence of CeO_2 NPs in the system increased the activity of the phosphatase. It has been established that enzyme activities such as amylase, acid phosphatase, catalase and urease increase significantly when the soil samples are treated with Fe_3O_4 NPs (Fang et al., 2012). It has also been established that iron oxide magnetic nanoparticles (IOMNPs) promote soil urease and invertase activities, and the possible reason for which is the change of the microbial community in the soil (He et al., 2011). Studies have shown that CeO_2 NPs could be applied to prevent retinal disorders (Silva, 2006), to elongate cell lifespan by protecting human normal cells from radiation (Tarnuzzer et al., 2005), and to enhance adult rat spinal cord neuron survival (Das et al., 2007). Based upon those benefits of CeO_2 NPs, it is possible that the stimulation effect of CeO_2 NPs on phosphatase activity may be caused by a shift in the microbial community to that of the phosphatase-associated microbes, as well as an increase in both their census and in vitality. However, further study is needed to elucidate the detailed mechanism of the promotion phenomenon between CeO_2 NPs and phosphatase.

The length of time that soil enzymes are exposed to the nanoparticles is also an important influence upon enzyme activities. A comparison of the first harvest event with the second and third events showed a continuously decrease in different concentration treatments with a corresponding inhibition or promotion of NPs. This decrease was particularly prevalent for the third harvest with some of the enzyme activities impervious to the influence of the concentration variance. In a study of nano-scale zerovalent iron (nZVI), the dehydrogenase activity was observed to increase greatly during a seven day testing period, from day 1 to day 7, which was interpreted as either a promoting effect on the microbial population or an assay artifact (Cullen et al., 2011). In the study of the promoting effect on dehydrogenase in soil type SL1, Jośko et al. (2014) noted a decrease with an increase in the contact time with ZnO NPs, which was consistent with the results for phosphatase activity. A longer exposure time was found to provide more opportunities for soil components, specifically clay particles and NOM, to interact with nanoparticles. This process in turn may immobilize NPs by adsorption and lower the bioavailability of NPs that come in contact with microbes, therefore reducing the toxicity. Regarding the ability of the soil microorganisms to metabolize and tolerate NPs, in addition to the self-protection mechanism and rapid adaptation to a changing environment through regeneration and horizontal gene transfer may also reasonably explain the reduced toxicity of NPs over time (Allison and Martiny, 2008; Dinesh et al., 2012; Meyer et al., 2004). These reduced inhibition and stimulating effects on selected enzyme activities with longer contact time with CeO_2 NPs could summarize to be a

possible lower bioavailability of CeO_2 NPs along with a resilient and resistant microbial response.

Comparing the results between the cut and non-cut groups, the enzyme activities decreased in cut groups at the second harvest for urease and phosphatase and at the third harvest for β-glucosidase. Similarly, in their analysis after wheat harvest, Du et al. observed a great reduction in enzyme (protease, catalase and peroxidase) activities (Du et al., 2011). The results also agreed with a study from Guitian and Bardgett (2000), in which the three tested grass species exhibited their highest microbial activities in the uncut control groups compared to the other two cut groups, respectively. Wheatgrass was chosen because it added a level of variability and complexity to the system compared to bare soil, and was also deemed a nutritious food source in forms of juice and powder (Wigmore, 1985). Such uses however, may cause adverse health effects if wheatgrass uptake of CeO_2 was observed. Although the primary focus of this study involved examining soil enzyme activity, the authors recommend a future study to determine how the traits of various plants may affect CeO_2 uptake.

5. Conclusion

CeO_2 NPs were found to influence soil enzyme activities in terms of enzyme type, dose treatment, contact length and cut type. Both inhibition and promotion effects were observed among the three enzymes tested, with urease and β-glucosidase exhibiting inhibition and phosphatase revealing stimulation under the treatment with CeO_2 NPs. The inhibition effect was deemed to be the accumulation of ROS that damaged the microbial

cells, while the stimulation effect on phosphatase was assumed to be a shift in microbial community, in addition to the antioxidant property of CeO_2 NPs that could improve the cell lifespan and vitality. The reduction in toxicity and promotion effects over time along the three harvest events was hypothesized to be a lower bioavailability of NPs and a microbial adaption and evolutionary process.

6. Tables and Figures

Table 2.1 Physicochemical properties of soil mixture.

		Soil Mixture
pH		5.7
Organic Material (%)		5.4
CEC (meg/100g)		17.7
Elements and Ions	Nitrate-N (ppm)	144
	Phosphorus (ppm)	139.5
	Potassium (ppm)	608.5
	Calcium (ppm)	1827.5
	Magnesium (ppm)	253.5
	Zinc (ppm)	18.55
	Manganese (ppm)	33.5
	Boron (ppm)	1.1
	Copper (ppm)	0.75
	Sodium (ppm)	123
	Cerium (ppm)	0.148

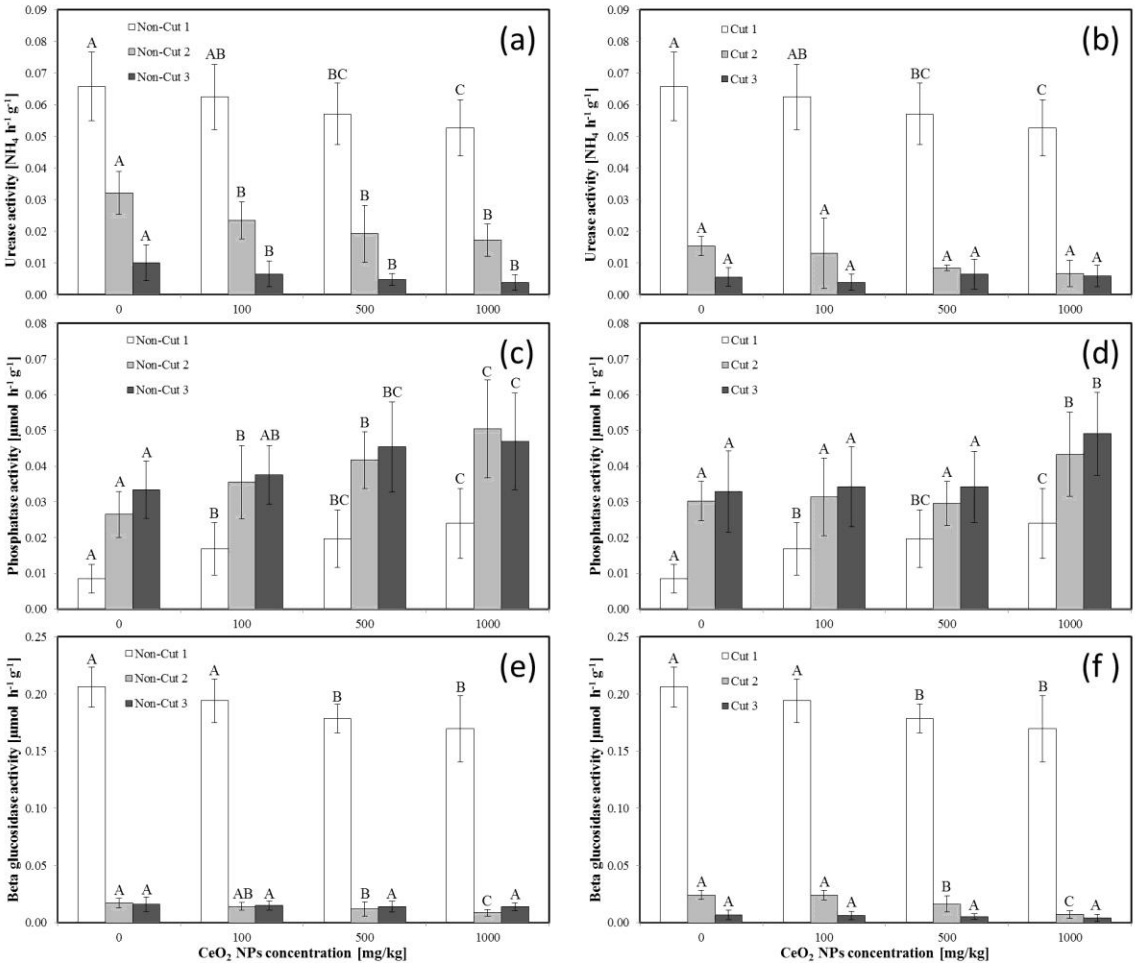

Figure 2.1 Enzymatic activity of urease as non-cut and cut groups (a, b), phosphatase as non-cut and cut groups (c, d), β -glucosidase as non-cut and cut group (e, f) under different concentrations of CeO_2 NPs and harvest periods. Error bars represent the standard deviation of the mean. The upper letters (A, B, C) mean statistically significant differences ($P \geq 0.05$) among concentrations.

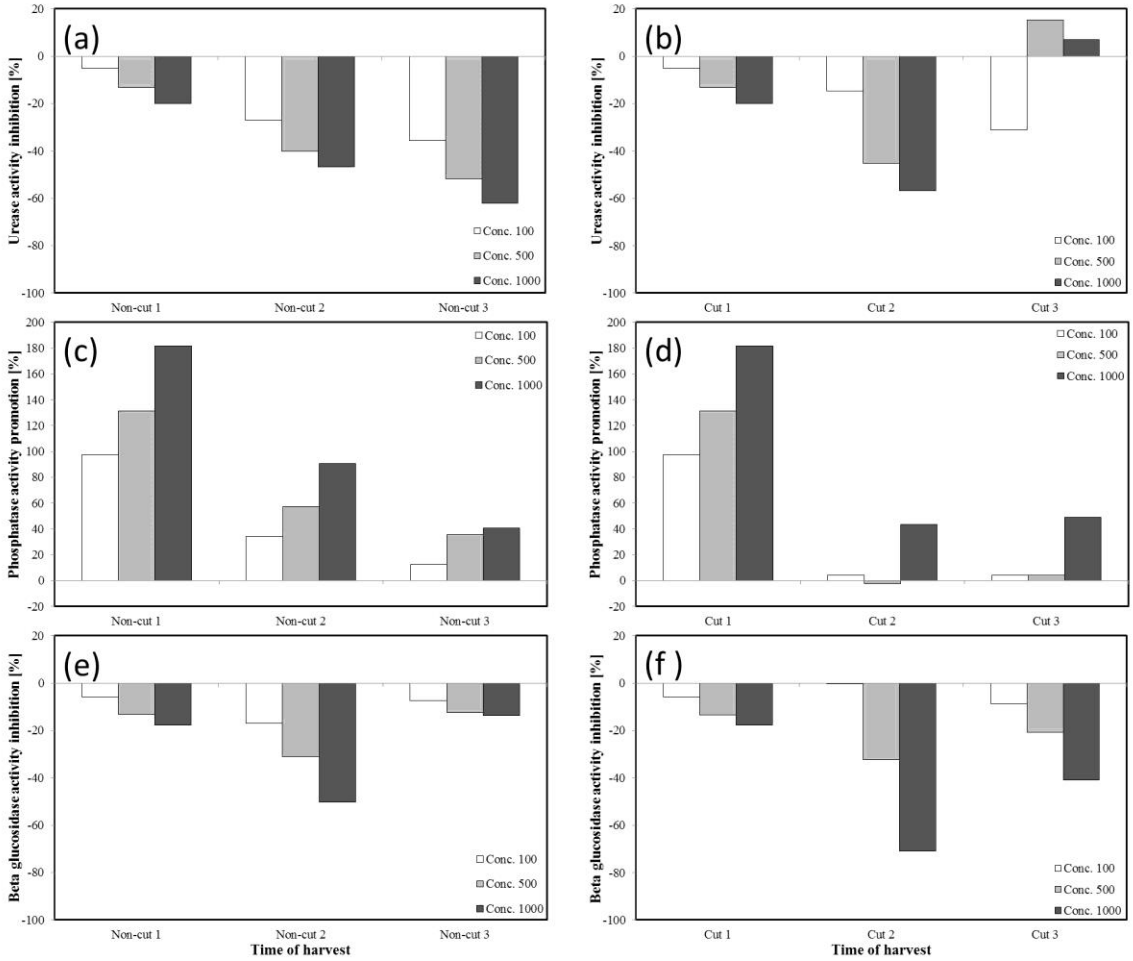

Figure 2.2 Influence of CeO_2 nanoparticles concentration and harvest times on urease activity as non-cut and cut groups (a, b), phosphatase activity as non-cut and cut groups (c, d), β –glucosidase activity as non-cut and cut group (e, f).

7. Acknowledgments

We wish to convey our appreciation to Clemson University for supporting this work and to Dr. Yi Zheng for use of the microplate reader required for conducting these experiments. We thank Dr. Yvan Capowiez, Editor-in-Chief of Geoderma, and the two anonymous reviewers for their thoughtful and constructive comments to improve our manuscript.

8. References

Allison, S., 2001a. Urease protocol. http://web.stanford.edu/group/Vitousek/Urease.pdf. (September 21, 2016)

Allison, S., 2001b. Enzyme assays for fresh litter and soil adapted from Bob Sinsabaugh lab, 1994. http://web.stanford.edu/group/Vitousek/enzymes2001.pdf. (September 21, 2016)

Allison, S.D., Martiny, J.B.H., 2008. Resistance, resilience, and redundancy in microbial communities. Proc. Natl. Acad. Sci. 105, 11512–11519. doi:10.1073/pnas.0801925105

Antisari, L.V., Carbone, S., Gatti, A., Vianello, G., Nannipieri, P., 2013. Toxicity of metal oxide (CeO_2, Fe_3O_4, SnO_2) engineered nanoparticles on soil microbial biomass and their distribution in soil. Soil Biol. Biochem. 60, 87–94. doi:10.1016/j.soilbio.2013.01.016

Antolín, M.C., Muro, I., Sánchez-Díaz, M., 2010. Application of sewage sludge improves growth, photosynthesis and antioxidant activities of nodulated alfalfa plants under

drought conditions. Environ. Exp. Bot. 68, 75–82. doi:10.1016/j.envexpbot.2009.11.001

Aon, M.A., Colaneri, A.C., 2001. II. Temporal and spatial evolution of enzymatic activities and physico-chemical properties in an agricultural soil. Appl. Soil Ecol. 18, 255–270. doi:10.1016/S0929-1393(01)00161-5

Bae, E., Park, H.J., Lee, J., Kim, Y., Yoon, J., Park, K., Choi, K., Yi, J., 2010. Bacterial cytotoxicity of the silver nanoparticle related to physicochemical metrics and agglomeration properties. Environ. Toxicol. Chem. 29, 2154–2160. doi:10.1002/etc.278

Bandick, A.K., Dick, R.P., 1999. Field management effects on soil enzyme activities. Soil Biol. Biochem. 31, 1471–1479. doi:10.1016/S0038-0717(99)00051-6

Bandyopadhyay, S., Peralta-Videa, J.R., Plascencia-Villa, G., José-Yacamán, M., Gardea-Torresdey, J., 2012. Comparative toxicity assessment of CeO_2 and ZnO nanoparticles towards Sinorhizobium meliloti, a symbiotic alfalfa associated bacterium: Use of advanced microscopic and spectroscopic techniques. J. Hazard. Mater. 241, 379–386. doi:10.1016/j.jhazmat.2012.09.056

Barton, L.E., Auffan, M., Olivi, L., Bottero, J.Y., Wiesner, M.R., 2015. Heteroaggregation, transformation and fate of CeO_2 nanoparticles in wastewater treatment. Environ. Pollut. 203, 122–129. doi:10.1016/j.envpol.2015.03.035

Blaise, C., Gagné, F., Férard, J.F., Eullaffroy, P., 2008. Ecotoxicity of selected nano-materials to aquatic organisms. Environ. Toxicol. 23, 591–598.

Blaser, S.A., Scheringer, M., Macleod, M., Hungerbühler, K., 2008. Estimation of

cumulative aquatic exposure and risk due to silver: Contribution of nano-functionalized plastics and textiles. Sci. Total Environ. 390, 396–409. doi:10.1016/j.scitotenv.2007.10.010

Casals, E., Vázquez-Campos, S., Bastús, N.G., Puntes, V., 2008. Distribution and potential toxicity of engineered inorganic nanoparticles and carbon nanostructures in biological systems. TrAC Trends Anal. Chem. 27, 672–683. doi:10.1016/j.trac.2008.06.004

Cassee, F.R., van Balen, E.C., Singh, C., Green, D., Muijser, H., Weinstein, J., Dreher, K., 2011. Exposure, health and ecological effects review of engineered nanoscale cerium and cerium oxide associated with its use as a fuel additive. Crit. Rev. Toxicol. 41, 213–229. doi:10.3109/10408444.2010.529105

Chen, S., Edwards, C.A., Subler, S., 2003. The influence of two agricultural biostimulants on nitrogen transformations, microbial activity, and plant growth in soil microcosms. Soil Biol. Biochem. 35, 9–19. doi:10.1016/S0038-0717(02)00209-2

Chung, H., Son, Y., Yoon, T.K., Kim, S., Kim, W., 2011. The effect of multi-walled carbon nanotubes on soil microbial activity. Ecotoxicol. Environ. Saf. 74, 569–575. doi:10.1016/j.ecoenv.2011.01.004

Cullen, L.G., Tilston, E.L., Mitchell, G.R., Collins, C.D., Shaw, L.J., 2011. Assessing the impact of nano- and micro-scale zerovalent iron particles on soil microbial activities: Particle reactivity interferes with assay conditions and interpretation of genuine microbial effects. Chemosphere 82, 1675–1682.

doi:10.1016/j.chemosphere.2010.11.009

Dahle, J.T., Arai, Y., 2015. Environmental geochemistry of cerium: Applications and toxicology of cerium oxide nanoparticles. Int. J. Environ. Res. Public Health 12, 1253–1278. doi:10.3390/ijerph120201253

Das, M., Patil, S., Bhargava, N., Kang, J.F., Riedel, L.M., Seal, S., Hickman, J.J., 2007. Auto-catalytic ceria nanoparticles offer neuroprotection to adult rat spinal cord neurons. Biomaterials 28, 1918–1925. doi:10.1016/j.biomaterials.2006.11.036

Dick, R.P., Pankhurst, C., Doube, B.M., Gupta, V.V.S., 1997. Soil enzyme activities as integrative indicators of soil health. Biol. Indic. soil Heal. 121–156.

Dimkpa, C.O., 2014. Can nanotechnology deliver the promised benefits without negatively impacting soil microbial life? J. Basic Microbiol. 54, 889–904. doi:10.1002/jobm.201400298

Dinesh, R., Anandaraj, M., Srinivasan, V., Hamza, S., 2012. Engineered nanoparticles in the soil and their potential implications to microbial activity. Geoderma 173, 19–27. doi:10.1016/j.geoderma.2011.12.018

Du, W., Sun, Y., Ji, R., Zhu, J., Wu, J., Guo, H., 2011. TiO_2 and ZnO nanoparticles negatively affect wheat growth and soil enzyme activities in agricultural soil. J. Environ. Monit. 13, 822–828. doi:10.1039/c0em00611d

EPA, 2009. Toxicological review of cerium oxide and cerium compounds. https://cfpub.epa.gov/ncea/risk/recordisplay.cfm?deid=214572&CFID=65631881&CFTOKEN=83694203. (September 21, 2016)

Fang, G., Si, Y., Tian, C., Zhang, G., Zhou, D., 2012. Degradation of 2,4-D in soils by

Fe_3O_4 nanoparticles combined with stimulating indigenous microbes. Environ. Sci. Pollut. Res. 19, 784–793. doi:10.1007/s11356-011-0597-y

Fang, X., Yu, R., Li, B., Somasundaran, P., Chandran, K., 2010. Stresses exerted by ZnO, CeO_2 and anatase TiO_2 nanoparticles on the Nitrosomonas Europaea. J. Colloid Interface Sci. 348, 329–334. doi:10.1016/j.jcis.2010.04.075

Frenk, S., Ben-Moshe, T., Dror, I., Berkowitz, B., Minz, D., 2013. Effect of metal oxide nanoparticles on microbial community structure and function in two different soil types. PLoS One 8, e84441. doi:10.1371/journal.pone.0084441

Gajjar, P., Pettee, B., Britt, D.W., Huang, W., Johnson, W.P., Anderson, A.J., 2009. Antimicrobial activities of commercial nanoparticles against an environmental soil microbe, Pseudomonas putida KT2440. J. Biol. Eng. 3, 1. doi:10.1186/1754-1611-3-9

Gardea-Torresdey, J.L., Rico, C.M., White, J.C., 2014. Trophic transfer, transformation, and impact of engineered nanomaterials in terrestrial environments. Environ. Sci. Technol. 48, 2526–2540. doi:10.1021/es4050665

Gogos, A., Knauer, K., Bucheli, T.D., 2012. Nanomaterials in plant protection and fertilization: Current state, foreseen applications, and research priorities. J. Agric. Food Chem. 60, 9781–9792. doi:10.1021/jf302154y

Gottschalk, F., Nowack, B., 2011. The release of engineered nanomaterials to the environment. J. Environ. Monit. 13, 1145–1155.

Gottschalk, F., Sun, T., Nowack, B., 2013. Environmental concentrations of engineered nanomaterials: Review of modeling and analytical studies. Environ. Pollut. 181,

287–300. doi:10.1016/j.envpol.2013.06.003

Guitian, R., Bardgett, R.D., 2000. Plant and soil microbial responses to defoliation in temperate semi-natural grassland. Plant Soil 220, 271–277. doi:10.1023/A:1004787710886

Handy, R.D., Owen, R., Valsami-Jones, E., 2008a. The ecotoxicology of nanoparticles and nanomaterials: Current status, knowledge gaps, challenges, and future needs. Ecotoxicology 17, 315–325. doi:10.1007/s10646-008-0206-0

Handy, R.D., Von der Kammer, F., Lead, J.R., Hassellöv, M., Owen, R., Crane, M., 2008b. The ecotoxicology and chemistry of manufactured nanoparticles. Ecotoxicology 17, 287–314. doi:10.1007/s10646-008-0199-8

Hänsch, M., Emmerling, C., 2010. Effects of silver nanoparticles on the microbiota and enzyme activity in soil. J. Plant Nutr. Soil Sci. 173, 554–558. doi:10.1002/jpln.200900358

He, S., Feng, Y., Ren, H., Zhang, Y., Gu, N., Lin, X., 2011. The impact of iron oxide magnetic nanoparticles on the soil bacterial community. J. Soils Sediments 11, 1408–1417. doi:10.1007/s11368-011-0415-7

HEI, 2001. Research report: evaluation of human health risk from cerium added to diesel fuel. Research Communication 9. https://www.healtheffects.org/system/files/Cerium.pdf. (September 21, 2016)

Henneberry, M.O., Engel, G., Grayhack, J.T., 1979. Acid phosphatase. Urol. Clin. North Am. 6, 629–641.

Jemec, A., Drobne, D., Remskar, M., Sepcić, K., Tisler, T., 2008. Effects of ingested

nano-sized titanium dioxide on terrestrial isopods (Porcellio scaber). Environ. Toxicol. Chem. 27, 1904–1914. doi:10.1897/08-036.1

Jin, L., Son, Y., Yoon, T.K., Kang, Y.J., Kim, W., Chung, H., 2013. High concentrations of single-walled carbon nanotubes lower soil enzyme activity and microbial biomass. Ecotoxicol. Environ. Saf. 88, 9–15. doi:10.1016/j.ecoenv.2012.10.031

Jośko, I., Oleszczuk, P., Futa, B., 2014. The effect of inorganic nanoparticles (ZnO, Cr_2O_3, CuO and Ni) and their bulk counterparts on enzyme activities in different soils. Geoderma 232, 528–537. doi:10.1016/j.geoderma.2014.06.012

Keller, A.A., Lazareva, A., 2014. Predicted releases of engineered nanomaterials: from global to regional to local. Environ. Sci. Technol. Lett. 1, 65–70. doi:10.1021/ez400106t

Keller, A.A., McFerran, S., Lazareva, A., Suh, S., 2013. Global life cycle releases of engineered nanomaterials. J. Nanoparticle Res. 15, 1–17.

Kiemnec, G., Larson, L.L., Grammon, A., 2003. Diffuse knapweed and bluebunch wheatgrass seedling growth under stress. J. range Manag. 65–67.

Kim, S., Kim, J., Lee, I., 2011. Effects of Zn and ZnO nanoparticles and Zn^{2+} on soil enzyme activity and bioaccumulation of Zn in Cucumis sativus. Chem. Ecol. 27, 49–55.

Kizilkaya, R., Bayrakli, B., 2005. Effects of N-enriched sewage sludge on soil enzyme activities. Appl. Soil Ecol. 30, 192–202. doi:10.1016/j.apsoil.2005.02.009

Klaine, S.J., Alvarez, P.J.J., Batley, G.E., Fernandes, T.F., Handy, R.D., Lyon, D.Y.,Mahendra, S., McLaughlin, M.J., Lead, J.R., 2008. Nanomaterials in the

environment: behavior, fate, bioavailability, and effects. Environ. Toxicol. Chem. 27, 1825–1851.

Lee, S., Lee, J., Kim, K., Sim, S.J., Gu, M.B., Yi, J., Lee, J., 2009. Eco-toxicity of commercial silver nanopowders to bacterial and yeast strains. Biotechnol. Bioprocess Eng. 14, 490–495. doi:10.1007/s12257-008-0254-6

Limbach, L.K., Bereiter, R., Müller, E., Krebs, R., Gälli, R., Stark, W.J., 2008. Removal of oxide nanoparticles in a model wastewater treatment plant: Influence of agglomeration and surfactants on clearing efficiency. Environ. Sci. Technol. 42, 5828–5833. doi:10.1021/es800091f

Lovern, S.B., Klaper, R., 2006. Daphnia magna mortality when exposed to titanium dioxide and fullerene (C_{60}) nanoparticles. Environ. Toxicol. Chem. 25, 1132–1137. doi:10.1897/05-278r.1

Lovern, S.B., Strickler, J.R., Klaper, R., 2007. Behavioral and physiological changes in Daphnia magna when exposed to nanoparticle suspensions (titanium dioxide, nano-C_{60}, and C $_{60}$HxC_{70}Hx). Environ. Sci. Technol. 41, 4465–4470. doi:10.1021/es062146p

Meyer, A.F., Lipson, D.A., Martín, A.P., Schadt, C.W., Schmidt, S.K., 2004. Molecular and metabolic characterization of cold-tolerant alpine soil pseudomonas sensu stricto. Appl. Environ. Microbiol. 70, 483–489. doi:10.1128/AEM.70.1.483-489.2004

Pan, B., Xing, B., 2010. Manufactured nanoparticles and their sorption of organic chemicals, in: Advances in Agronomy. Elsevier Inc., pp. 137–181.

doi:10.1016/S0065-2113(10)08003-X

Pelletier, D.A., Suresh, A.K., Holton, G.A., McKeown, C.K., Wang, W., Gu, B., Mortensen, N.P., Allison, D.P., Joy, D.C., Allison, M.R., Brown, S.D., Phelps, T.J., Doktycz, M.J., 2010. Effects of engineered cerium oxide nanoparticles on bacterial growth and viability. Appl. Environ. Microbiol. 76, 7981–7989. doi:10.1128/AEM.00650-10

Peyrot, C., Wilkinson, K.J., Desrosiers, M., Sauvé, S., 2014. Effects of silver nanoparticles on soil enzyme activities with and without added organic matter. Environ. Toxicol. Chem. 33, 115–125. doi:10.1002/etc.2398

Piccinno, F., Gottschalk, F., Seeger, S., Nowack, B., 2012. Industrial production quantities and uses of ten engineered nanomaterials in Europe and the world. J. Nanoparticle Res. 14, 1–11.

Roco, M.C., 2011. The long view of nanotechnology development: the National Nanotechnology Initiative at 10 years. J. Nanoparticle Res. 13, 427–445. doi:10.1007/s11051-010-0192-z

Roh, J.Y., Park, Y.K., Park, K., Choi, J., 2010. Ecotoxicological investigation of CeO_2 and TiO_2 nanoparticles on the soil nematode Caenorhabditis elegans using gene expression, growth, fertility, and survival as endpoints. Environ. Toxicol. Pharmacol. 29, 167–172. doi:10.1016/j.etap.2009.12.003

Shin, Y.J., Kwak, J.I., An, Y.J., 2012. Evidence for the inhibitory effects of silver nanoparticles on the activities of soil exoenzymes. Chemosphere 88, 524–529. doi:10.1016/j.chemosphere.2012.03.010

Silva, G.A., 2006. Nanomedicine - Seeing the benefits of ceria. Nat. Nanotechnol. 1, 92–94. doi:Doi 10.1038/Nnano.2006.111

Sinsabaugh, R.L., Antibus, R.K., Linkins, A.E., McClaugherty, C.A., Rayburn, L., Repert, D., Weiland, T., Weiland, T., 1993. Wood decomposition: nitrogen and phosphorus dynamics in relation to extracellular enzyme activity. Ecology 74, 1586–1593.

Suppan, S., 2013. Nanomaterials in soil*: Our future food chain?* Institute for Agriculture and Trade Policy

Tarnuzzer, R.W., Colon, J., Patil, S., Seal, S., 2005. Vacancy engineered ceria nanostructures for protection from radiation-induced cellular damage. Nano Lett. 5, 2573–2577. doi:10.1021/nl052024f

Tong, Z., Bischoff, M., Nies, L., Applegate, B., Turco, R.F., 2007. Impact of fullerene (C_{60}) on a soil microbial community. Environ. Sci. Technol. 41, 2985–2991. doi:10.1021/es061953l

Unrine, J., Bertsch, P., Hunyadi, S., 2008. Bioavailability, trophic transfer, and toxicity of manufactured metal and metal oxide nanoparticles in terrestrial environments, in: Grassian, V. (Ed.), Nanoscience and Nanotechnology: Environmental and Health Impacts. pp. 345–366.

Velzeboer, I., Hendriks, A.J., Ragas, A.M., Van De Meent, D., 2008. Aquatic ecotoxicity tests of some nanomaterials. Environ. Toxicol. Chem. 27, 1942–1947. doi:0730-7268

Wang, H., Wick, R.L., Xing, B., 2009. Toxicity of nanoparticulate and bulk ZnO, Al_2O_3

and TiO_2 to the nematode Caenorhabditis elegans. Environ. Pollut. 157, 1171–1177. doi:10.1016/j.envpol.2008.11.004

Wigmore, A., 1985. The wheatgrass book. Penguin.

Xu, C., Peng, C., Sun, L., Zhang, S., Huang, H., Chen, Y., Shi, J., 2015. Distinctive effects of TiO_2 and CuO nanoparticles on soil microbes and their community structures in flooded paddy soil. Soil Biol. Biochem. 86, 24–33. doi:10.1016/j.soilbio.2015.03.011

Zantua, M.I., Bremner, J.M., 1977. Stability of urease in soils. Soil Biol. Biochem. 9, 135–140. doi:10.1016/0038-0717(77)90050-5

Zhang, H., He, X., Zhang, Z., Zhang, P., Li, Y., Ma, Y., Kuang, Y., Zhao, Y., Chai, Z., 2011. Nano-CeO_2 exhibits adverse effects at environmental relevant concentrations. Environ. Sci. Technol. 45, 3725–3730. doi:10.1021/es103309n

Zimmer, M., 2000. Molecular mechanics evaluation of the proposed mechanisms for the degradation of urea by urease. J. Biomol. Struct. Dyn. 17, 787–797. doi:10.1080/07391102.2000.10506568

CHAPTER THREE

DYNAMICS OF FLUID INTERFACES AND NONEQUILIBRIUM AND PREFERENTIAL FLOW IN THE VADOSE ZONE: IMPACT OF MICROBIAL EXUDATES

1. Introduction

The infiltration process is a most important factor within the hydrological cycle as it filters water from both the atmosphere and the ground surface into the soil, which in turn revives the underground ecosystem through a recharged ground water table to ensure the continuity of the cycle. A combination of gravity and capillarity forces act upon the water and upon entry into the soil pores with gravity always acting vertically and with the capillary forces channeling the water horizontally (Gray and Norum, 1967). Derived in 1931 by Lorenzo A. Richards, the Richards equation is used to determine water flow in the vadose zone under constant temperature from Darcy's law and the conservation of mass. It is expressed as:

$$\frac{\partial \theta}{\partial t} = \frac{\partial}{\partial Z}\left[K(\theta)\frac{d\psi(\theta)}{d\theta}\frac{\partial \theta}{\partial z}\right] - \frac{\partial K(\theta)}{\partial z} = \frac{\partial}{\partial z}\left[D(\theta)\frac{\partial \theta}{\partial z}\right] - \frac{\partial K(\theta)}{\partial z} \qquad (1)$$

where θ represents the volumetric water content in soil, t the time, z the vertical axis pointing downward indicating positive, K the soil hydraulic conductivity, Ψ the soil water potential, and D the soil water diffusivity. This highly nonlinear problem makes the analytical and numerical solutions to the Richards equation typically non-unique (Celia et al., 1990). Many simplifications and approximations to the Richards equation have been proposed (e.g. Bras, 1990; Smith et al., 1993; Waechter and Philip, 1985).

Water flow during the infiltration processes in soil systems is either uniform, with wetting fronts flowing in parallel to the soil surface level; or non-uniform, with wetting fronts flowing irregularly (Green and Ampt, 1911). In a non-uniform flow, water movement in some areas of the unsaturated subsurface is faster and more intense than in others. Macropore flow, unstable flow, funnel flow and preferential flow are a few of the characteristic non-uniform flows that may occur. Of these, preferential flow refers to the movement of water in addition to the solutes in a non-uniform flow and is independent from common conditions that characterize soils in various locations (Andreini and Steenhuis, 1990; Baveye et al., 1998; Dekker and Ritsema, 1996; Doerr et al., 2007, 2006). The occurrence of fingering flows, one form of preferential flows, which frequently occurs in coarse media can occur (i) with the entrapment of air during the movement of the wetting front, (ii) the movement through water-repellent soils, (iii) the process of continuous non-ponding infiltration, and (iv) among layered materials with different textures (Baker and Hillel, 1990; Diment and Watson, 1985; Du et al., 2001; Glass et al., 1991, 1990, 1989a, 1989b, 1989c; Hill and Parlange, 1972; Hillel and Baker, 1988; Parlange and Hill, 1976; Philip, 1975a, 1975b; Raats, 1973; Selker et al., 1992; Tamai et al., 1987; Yao and Hendrickx, 1996, 2001). The surface tension and contact angle are the two parameters most commonly examined that occur in an infiltration process (Yuan and Lee, 2013).

The formation of preferential flow may derive either directly or indirectly from various biological influences. Although plant root zones induce water into the soil, microorganisms and their secreted compounds can change the hydraulic conductivity by

modifying the soil porosity and inducing water repellency, which then forms preferential flow paths (Morales et al., 2010). These preferential flow paths of a soil profile can then form a saturated distribution zone near the top surface and an underlying conveyance zone with the fingering flow paths (Kim et al., 2005; Steenhuis et al., 1994). These unstable wetting fronts for unstable flow then splits the original horizontal profiles into fingering flow paths that can possibly cause a leaching of contaminants via the soil into the groundwater (Bauters et al., 2000; Doerr et al., 2007; Hendrickx and Flury, 2001; Wang et al., 2000). In addition, unexpected dry and wet soil patches from fingering flow paths can negatively affect microbial populations and plant growth (Morales et al., 2010). For example, the agrochemicals and wetting agents (surfactants) regularly applied to golf course greens can rapidly move through the subsurface from a preferential flow (Kostka, 2000; Morales et al., 2010).

Soil moisture is an integral component concerning the support of biogeochemical processes as nutrient cycles, and a catalyst for microbial and plant activities (Wang et al., 2015). Soil modification by microorganisms and plant roots creates preferential flow, which in turn facilitates the microbial and plant activity by supplying more oxygen, moisture content, available nutrients, and different dissolved substrates along the wetted flow path. The soil-water dynamics are complex due to the heterogeneity in soil media from the nonuniform spatial distribution of microorganisms and plant roots, different soil structures, numerous interrelated biogeochemical reactions, spatial and temporal variability, and the scaling factor for hydrological processes (Ettema and Wardle, 2002; Morales et al., 2010).

Microorganisms growing in the soil tend to accumulate low molecular weight organic molecules, also known as osmolytes. The semi-permeability of membranes of these microorganisms causes a release of the intracellular solutes as exudates which in turn preserves their osmotic potential with the surrounding medium. Although the exudate production between microorganisms varies, this microbial response is a useful strategy to prevent cell lysis and death caused by changes in soil water content (Boot et al., 2013; Griffin, 1981; Halverson et al., 2000; Kieft et al., 1987; Potts, 1994; Wang et al., 2015). It has been determined that plant exudates released by roots can function as surfactants and change surface tension of soil solutions, which in turn alters the hydraulic conductivity and water flow around the rhizosphere (Passioura, 1988; Read et al., 2003; Read and Gregory, 1997). As surface-active organic compounds, surfactants can alter both surface tension of liquids and contact angle at the solid-liquid interface, which can further influence both the water flow and the potential transport of contaminants in the vadose zone (Bashir et al., 2008; Karagunduz et al., 2015). However, little research has been undertaken to examine the influence of different microbial exudates on water infiltration processes into the vadose zone. Catechol is one compound produced by certain bacteria (e.g. *Escherichia coli*) that can be synthesized by feeding those microbes on glucose and as intermediates during the biodegradation processes of aromatic compounds (e.g. phenol) (Draths and Frost, 1995; Li et al., 2005; Nair et al., 2008). Riboflavin (or vitamin B_2), which is naturally produced by many microorganisms, including *Candida famata*, *Bacillus subtilis*, and lactic acid bacteria is a second compound that can be treated as a microbial exudate (Bacher et al., 2001; Perkins et al.,

1999; Perkins and Pero, 1993; Schallmey et al., 2004; Stahmann et al., 2000; Thakur et al., 2016).

First used in by Hoa in 1981 to measure water the content in two-dimensional unsaturated sandy porous media the Light Transmission Method (LTM) is ideal for studying the infiltration process without disturbing the porous media system. This non-invasive imaging technique is inexpensive, fast responding and and provides high resolution with a mininum of acquisition time (Darnault et al., 1998; Werth et al., 2010). In order to acquire available data, a transparent (thin enough to be two dimensional) system that enables visible light to transmit through is needed. For data capture device, charge-coupled device (CCD) camera is commonly used for acceptable resolution purpose (Werth et al., 2010). The light intensity data separated from the original RGB image can be converted to the percentage of water saturation based on respective calibration equation. As a result, profiles of water distribution of wetting front and fingered flow during infiltration process can be obtained and then analyzed for flow characteristics.

Very little study has been undertaken to examine the infiltration process in porous media using the LTM, and even less to elucidate the influence of microbial exudate on the flow process. Although plant exudates act as surfactants to influence water flow, the effect of microbial exudates upon the infiltration process is unknown. Therefore, a random rain event, rather than point source was simulated to mimic natural conditions, and to use LTM to investigate the effect of these microbial on preferential flow with

different concentrations, which relate to different concentrations of biomass when applying real microbes.

The primary objective of this research study entailed an investigation of how different microbial exudates with varying concentrations alter the infiltration process in an unsaturated sand system and the distribution of the soil moisture content. Specifically, the microbial exudates catechol and riboflavin were examined to determine any influence of flow in porous media. The surface tension and the contact angle were dynamically monitored to obtain the interfacial properties of exudate solutions, and the infiltration experiments were conducted in a homogeneous and initially dry porous media in a two-dimensional (2D) tank. A light transmission method (LTM) with high spatial and temporal resolution was used to construct the flow patterns and to visualize the water content distribution followed by the use of MATLAB to process the imaging and data analyses.

2. Material and Methods

2.1 Microbial exudates solution preparation

Two solutions of microbial exudate were simulated using catechol and riboflavin, the molar concentrations of which were 10, 100, 500, and 1000 μM, respectively. For the catechol (≥99.5%, Sigma-Aldrich, St. Louis, MO) solution, 1.10, 11.01, 55.05, and 110.10 mg of catechol powder were mixed with 0.01M of BDH ACS Grade NaCl (VWR International, Radnor, PA) solution. For the riboflavin (≥98%, Sigma-Aldrich, St. Louis, MO) solution, 3.76, 37.64, 188.18, and 376.36 mg of riboflavin powder were mixed with

0.01M of NaCl solution. Ultrapure deionized (DI) water with a resistivity of 18.2 MΩ•cm (Millipore Corporation, Billerica, MA) was used to limit any errors from impurities. Prior to measurements, all solutions were adjusted to pH of 4.80 ± 0.03 by adding 0.01M of HCl (36.5-38.0%, Sigma-Aldrich, St. Louis, MO) or 0.01M of BDH ACS Grade NaOH (VWR International, Radnor, PA) using a XL 500 pH meter (Fisher scientific, Waltham, MA).

2.2 Contact angle and surface tension

The FM40Mk2 EasyDrop model instrument was used to measure the contact angle (Krüss, Hamburg, Germany), and the EasyDrop complimentary Drop Shape Analysis software was used to process the detected data. A 5 μL drop of sample was excreted from a 1 mL Norm-Ject syringe (Fisher Scientific, Waltham, MA) with an attached needle to form a sessile drop on a glass slide that was continuously measured at 30 seconds increments when placed in front of a camera for 10 minutes. All samples were conducted in triplicate, and the results were recorded in Excel.

A Krüss and Dropshape Analysis apparatus with a needle of approximately 1.8 mm in diameter was then used to experimentally measure the surface tension. A pendant drop was formed from the tip of the needle and imaged by the camera to determine the interfacial tension measurement in mN/m. The parameters for embedding phase density (air in this case) and temperature were adjusted in the setting to 0.0012 g/cm^3 and 23°C for the surface tension measurements. Droplets from the sample solutions were measured at 30 second increments in front of the camera over five full minutes. All samples were also again conducted in triplicate, and the results were recorded in Excel.

2.2 Two-dimensional tank flow experiment

A two-dimensional tank with two plates constructed of scratch-resistant polycarbonate and an inner dimension of 30.2 cm × 1.2 cm × 30.8 cm (L×W×H) was used for the microbial exudate flow experiments. The bottom of the tank on which was layered four pieces of ceramic porous plates for permeability was inclined downwards to the left. Four evenly distributed drainage outlets and one additional outlet on the left corner were also placed within the tank. During flow experiments, a filter sheet was placed at the bottom to prevent sand clogging and for the proper solutions to drain. A picture of the 2D tank with setup is shown in Figure 1. ASTM C778 Graded sand with unground silica was used and the surplus was loaded into a handmade Y-shaped sand loader with a piece of cloth within, with the loader taped above the tank (U.S. Silica Company, Ottawa, IL). The cloth was then quickly removed from the tank to create a uniform packing of sand within the tank. The rest of the sand in the loader and the loader were then removed. To ensure a consistent density of sand, a plastic rod was used to tap the top edge of the tank several times to “settle” the top sand layer.

After the tank was loaded with sand, the microbial exudate solutions were pumped into the tank through a Model 77200-60 Easy-Load II peristaltic pump head (Masterflex, Gelsenkirchen, Germany) via a connecting tube at a constant flow rate of 10 mL/min. Solutions were continuously stirred during the experiment in their containers which were positioned on a MS3002S NewClassic balance (Mettler Toledo, Columbus, OH) to record the initial and final weights. The other end of tube was connected to an actuator, which moved back and forth at a constant speed above the tank. Two short tube

openings were suspended from the actuator, and solutions randomly dropped from either tube to simulate a random rainfall event with an infiltration velocity of 16.56 cm/hr into the sand system.

2.3 Visualization and light transmission method

The light transmission method was used to visualize the microbial exudate solution flow pattern within the 2D tank. A 0.6 m × 0.6 m square even-glow LED panel light fixture with natural white color and a maximum of 2,900 lumens (Super Bright LEDs, St. Louis, MO) was placed behind the 2D tank. The entire configuration was fully covered by a black plastic sheet except for the tank front surface to avoid extra light emanation from the side. A D5500 DSLR camera (Nikon, Tokyo, Japan) on a VTSL7200 72" tripod (Bower, Long Island City, NY) was placed in front of the tank at a distance to record the transmitted light through the sand column in the 2D tank with a constant flow of exudate solution. The camera setting was adjusted to “manual” to avoid overexposure with only the LED panel light activated when both pump and actuator started to function. The camera then began imaging automatically every 30 seconds until the bottom of the tank was saturated and then drained for at least five minutes. Each flow experiment was performed in duplicate.

2.4 Data and imaging analysis

For each flow experiment, four pictures representing different stages of the main finger formation, prior to reaching the tank’s bottom, were analyzed in addition to the original picture at a time of 0 minutes and a drainage picture for calibration purposes. MATLAB R2016a was used to process the pictures, specifically to convert RGB (red,

green and blue) files to the form in HSV (hue, saturation and intensity), where the intensity was solely used later. The imaging method yielded both a high spatial resolution by tracking the main finger formation and a constant temporal response at 30-second intervals. Both of the vertical and horizontal distribution profiles were analyzed along and across the main finger for each stage of its development. A 30 pixel-wide rectangle appearing as a vertical line was drawn through the middle of the main finger to provide a vertical water distribution profile along the length, with a second rectangle horizontally drawn across the main finger at 90% of its total length to provide a horizontal profile. Regression equations were calculated using a previously observed linear relationship between the water content and the image light intensity based on the initial and fully saturated images with water saturation degree of 0% and 100%, respectively (Darnault et al., 2001; Hoa, 1981). MATLAB was then used to code the regression equations to calculate the water saturation based on the captured intensity values of each finger.

3. Results

3.1. Contact angle and surface tension

3.1.1 Catechol

The contact angles for the catechol solutions that were continuously measured for 10 minutes at 30-second intervals are shown in Figure 3.2. The lowest concentration of 10 μM catechol solution with 0.01 M NaCl exhibited the highest contact angle among the four concentrations. An increase in the catechol concentration from 10 μM to 1000 μM reduced the contact angle from $75 \pm 2.82°$ to $69 \pm 3.52°$ at time 0 min successively. At

approximately 10 minutes, all contact angles decreased and slowly plateaued. The initial contact angle of 76.7 ± 1.61° in the 0.01 M NaCl control solution suddenly declined and finally exhibited a higher contact angle compared to the solutions with catechol added.

The measurements of surface tension for catechol solutions in Figure 3.3 show similar results between 72.5 mN/m to 74.5 mN/m within a period of 5-min. The initial surface tension for a 10 μM solution of catechol was greater than the 100 μM and 1000 μM solutions of catechol, with the lowest surface tension within the 500 μM solution. However, within five minutes, a slight fluctuation of surface tensions indicated no significant difference overall. Compared to the control solution of 0.01 M NaCl with the surface tension at 73.7 ± 0.04 mN/m, the 10 μM and 100 μM catechol solutions caused an increased in surface tension, whereas the 500 μM and 1000 μM solutions caused a decrease.

3.1.2 Riboflavin

The contact angles for the riboflavin solutions were monitored for 10 minutes at 30-second intervals, the results of which are shown in Figure 3.4. Of the four concentrations analyzed, the lowest contact angle was for the 10 μM concentration of riboflavin solution with 0.01 M NaCl at 0 min, and the solution with the 1000 μM concentration exhibited the highest value. The contact angle increased from 75.3 ± 0.70° to 80.3 ± 1.47° when the riboflavin concentration increased from 10 μM to 1000 μM, the rise of which was concentration-dependent and increased in order. When the time approached 10 minutes, all decreasing trends began to plateau, however. Although the initial contact angle of the 0.01 M NaCl control solution was greater than 10 and 100 μM

solutions, the overall trend was similar to the 10 μM of riboflavin solution in the later stage.

The surface tensions for riboflavin solutions were then measured continuously every 30 seconds for 5 minutes, which are shown in Figure 3.5, indicated a lower surface tension with higher riboflavin concentrations. These values fluctuated slightly, however, which failed to indicate any great differences within the range of 73.5 to 75 mN/m. The initial surface tension decreased from 74.6 $\pm$ 0.12 mN/m to 73.9 $\pm$ 0.25 mN/m when the riboflavin concentration increased from 10 μM to 1000 μM. The 0.01 M NaCl control solution exhibited the lowest surface tension during this five-minute interval, however.

3.1.3 Microbial exudate solutions versus control

The percentage difference in contact angle for catechol and riboflavin solutions compared to the control NaCl solution is shown in Figure 3.6. At concentration of 500 μM and 1000 μM, the two microbial exudates exhibited the opposite percentages compared to the baseline of control. For example, the contact angle for catechol solution was about 11% smaller than the control, while it was almost 13% greater than the control for riboflavin solution at 1000 μM.

Similarly, the percentage difference in surface tension for catechol and riboflavin solutions compared to the control is plotted in Figure 3.7. At concentration of 500 μM and 1000 μM, the two microbial exudates also showed opposite values, however the overall difference in percentage was not large compared to that in the contact angle. For example, at 500 μM, the catechol solution was -0.36% and the riboflavin solution was 0.68% different from the control.

3.2 Profile analysis of the finger development

The 2D tank visualizations of the flow experiments representing the microbial exudate dependent infiltration processes were subsequently displayed for water distribution profiles as original RGB pictures, extracted intensity figures, and water saturation percentage profiles. Detailed information about the finger numbers and characteristics are shown in Table 3.1.

3.2.1 Catechol

Catechol solutions with four different concentrations were analyzed along and across the main finger of the intensity and water saturation distribution profiles. These four successive stages, beginning at 5 min and ending prior to contact of the primary finger to the tank bottom are shown in their vertical profiles and respective concentrations (Figures 3.8(a) to 3.8(d)). It was determined, from a comparison of the main finger shapes between catechol concentrations that more small branches formed on the two sides of the finger formed at higher concentrations. The finger exhibiting the most tendrils was that observed within the 1000 μM catechol solution, while the sides were flat and smooth at the 10 μM solution. As the catechol concentration increased from 10 μM to 1000 μM, the water saturation percentage at the fingertip increased from approximately 70%, to 80%, to 90% and finally to full saturation. Two fingers were mostly formed among the four concentrations of catechol exudate solution. In terms of velocity of the main finger development, the finger velocity increased from 1.63 cm/min at concentration of 10 μM to 2.17 cm/min at concentration of 1000 μM in sequence. Regarding the NaCl control solution (Figure 3.8(e)), three fingers were formed, which

were mostly smooth at two sides, and the water saturation percentage at the fingertip was in a similar range with the 500 μM of catechol solution, roughly around 90%.

The horizontal profiles of the final stages for four concentrations of catechol as well as the control NaCl solution are collectively shown in Figure 3.9. The main finger width at the fingertip was widest for 10 μM catechol solution, which was 11.72 cm, and it decreased to a range of five to seven centimeters at higher concentrations. As for the control NaCl solution, the width was 8.4 cm at the fingertip. At 90% of the total length of the main fingers, the saturation percentage profiles suddenly increased and dropped at both sides where the solution failed to reach the sand matrix. The middle portion of the water saturation percentage profiles increased from approximately 70% to 80%, to 90% and to almost 100% as the catechol concentrations raised from 10 μM to 1000 μM, which was consistent with the vertical profiles.

3.2.2 Riboflavin

Four concentrations of riboflavin solutions were analyzed along and across the main finger beginning at 5 min and terminating when the main finger almost contacted with the bottom. The vertical profiles by concentrations for the four successive stages of finger formation, including their original RGB pictures, the corresponding intensity figures and the water saturation percentage distribution profiles, as well as the NaCl control for purposes of comparison are respectively shown in Figure 3.10. An analysis of the main finger shapes indicated a more bulbous main finger within an increase in riboflavin concentration from 10 μM to 500 μM. Further, the water saturation percentage also increased at the fingertip of the riboflavin solutions from 75% to 85% and to 90% as

the concentrations increased from 10 μM to 500 μM, with the exception of the 1000 μM solution (which decreased to 80%). Each of the four riboflavin concentrations also formed two fingers during which the velocity was the highest (2.07 cm/min) at 10 μM concentrations and decreased to 1.63 cm/min at 1000 μM concentrations. For a 1000 μM concentration of riboflavin solution, the slightly inclined main finger was relatively thinner compared to the fingers at lower concentrations, and it did not exhibit the highest water saturation percentage as the fingertip in the last stage. The highest percentage of water saturation in the NaCl control was approximately 90%, which was quite close to the 500 μM of the riboflavin solution.

The horizontal profiles for the final stages of the four concentrations of riboflavin and the control NaCl solutions are shown in Figure 3.11. The widest main finger width was 9.84 cm at 500 μM, with the width decreasing to 6.97 cm a 100 μM and to 6.66 cm at 10 μM. An approximate 75% of water saturation percentage was observed in the horizontal profiles for the 10 μM solution， and it increased to nearly 90% for the 500 μM solution and then decreased to 80% for the 1000 μM solution, which were consistent with the vertical profiles.

4. Discussion

Microbial exudate, as the first step in the simulation of a microbial effect, does affect the preferential flow through porous media. In this research, catechol and riboflavin were studied particularly as were the interfacial characteristics of contact angle

and surface tension, which played an important role in the analysis of the fingering process.

The study of interfacial characteristics of catechol and riboflavin provided the basic information for their linkage to preferential flow features. The opposite behaviors in contact angle in addition to different performances in surface tension induced various flow patterns for two exudate solutions among four concentrations at 10, 100, 500 and 1000 μM. The light transmission method was then used to correlate the light intensity to the water saturation percentage, which showed significant differences among the profiles.

In a porous medium, the preferential flow leads to finger-shaped wetted zone filled with water and solutes. The fingers in the initially dry medium formed wet cores with relatively high water content in contrast to their dry surroundings as initially described by Hill and Parlange (1972). The movement of the main fingers downwards, as indicated in the images, failed to disturb the widths of the finger cores for a short distance immediately behind the fingertip. This stasis was due to the drying process after the fingertip passed, and the reduction of the matric potential of that area that affected the medium sorptivity and prevented a rapid expansion of the fingers (Glass et al., 1989c). Similarly, an analysis of the relationship between the width and velocity of the finger determined that a higher flow rate led to a wider and faster moving finger (Glass, 1985). In this examination of the flow experiments under the same infiltration rate, the physical properties of the microbial exudate solutions were deemed the major cause of variability in the preferential flow paths (i.e. fingered flow), however. The sizes and shapes of the fingers and the water distribution profiles for all the 2D tank experiments provided the

most direct evidence of the catechol and riboflavin solutions that were analyzed. Each of the four concentrations of respective microbial exudate solution indicated distinct contact angles and surface tensions, all of which placed different stresses upon the infiltration process and finger formation.

The number of fingers observed in the results was similar for each chemical solution. Two fingers were mostly formed in the system with the vertical profiles for the main fingers exhibiting similar patterns. From top to bottom of the 2D tank, these main fingers often encompassed two zones, both of which differed from the theoretical finger profile described by Glass et al. (1989). An ideal finger has three zones of classification indicating a downward migration of the solutions in an initially dry medium. The conceptual profile transitioned from a zone with a constant moisture content of between 50% to 60% to that of an increasing gradient in water content, and which reached near or full saturated at the fingertip. Further, although only the transition and saturation zones were clearly observed in the vertical profiles for catechol and riboflavin solutions, all three zones were present in the NaCl control solution. The difference between the control solution and the exudate added solutions indicated a possible increase of water content in porous medium by the microbial exudate prior to saturation. It is now known that microbial excreted extracellular polymeric substance (EPS) can increase the holding capacity of soil water (Morales et al., 2010), which was consistent with the findings detailed here. Specifically, an application of EPS on soil particles showed an increase in soil-water contact angle and a great change in soil matric potential, which caused the formation of preferential flows (Bauters et al., 2000). Similarly, the use of commercially

prepared dextran and xanthan to model the microbial exudates of polysaccharides to analyze the soil structure and water transport indicated a reduction in water repellency of soils after the microbial exudate treatment (Czarnes et al., 2000). Clearly, these studies validated the effect of the microbial exudates on the infiltration process that was detailed in this study.

An analysis of the effect of concentration differences for each microbial exudate solution was also undertaken during the infiltration experiment. It is well known that the underground migration of contaminants is closely related to the properties and chemistries of the solution, meaning that the solute concentration, ionic strength and pH affect both the surface tension and contact angle (Bashir et al., 2009, 2008; Henry and Smith, 2002; Lord et al., 1997). Therefore, the Young-Laplace equation can be used to clearly express the relationship between the surface tension and the contact angle and capillary pressure at the pore scale. This equation is expressed as:

$$P_C = \frac{2\gamma \cos\theta}{r} \tag{2}$$

where P_C is the expression for capillary pressure, γ and θ are the surface tension and contact angle of a solution, respectively, and r is the radius of the pore size of medium (Lord et al., 1997).

To explain the action of the interfacial forces upon the solution's infiltration process, we assume a constant radius for pore size under various combinations of surface tension and contact angle. The capillary pressures will then correspondingly contribute to water flow and distribution changes across the porous medium, which finally results in diverse infiltration processes and finger shapes. Here, a decrease in contact angle at

higher concentrations of catechol solution likely increased the wettability of porous medium thus causing a greater protrusion of the solution into the dry matrix, and quickly reach conditions of near saturation. The slopes of the transition zone shown in vertical profiles increase with increasing catechol concentrations can reflect this faster water distribution rate. Based on these horizontal profiles for the catechol solutions under study, the water distribution profile at 90% of the total finger length of the highest catechol concentration of 1000 μM showed the greatest drops at two edges, the greatest constancy of water content in between and the narrowest width. As expressed in Equation 2 at 1000 μM of catechol solution for example, the largest cosine of the contact angle, which was given by the smallest contact angle value, multiplying by the second small surface tension nearly cancelled out its resulted capillary pressure change (Figure 3.2, 3.3). Therefore, the capillary pressure may not be the causative factor in the difference in finger development process among concentrations for catechol. A better water holding capacity induced by a catechol solution at higher concentration may be useful in explaining the greater wettability and water saturation percentage at fingertip and a reduction in drainage to the surrounding dry matrix (Figure 3.9). Here, the water holding capacity resulting from catechol may dominate the preferential flow patterns over the interactives forces that occur at the interfaces of soil-water solution and sand grain, and of soil-water solution and air.

An increase in contact angle that was observed with an increase in concentration of riboflavin indicated that more time was required within the medium to form a fully developed main finger due to decreased wettability. The difference in the slope of the

transition zone, the water content at the fingertip, and the horizontal water distribution profile between four riboflavin concentrations was not as apparent as in the catechol solutions (Figure 3.10). However, a slight increase in saturation percentage at the fingertip and in the overall finger width shown in riboflavin's vertical and horizontal profiles from 10 to 500 μM could still be observed, with an exception of 1000 μM where the finger might be affected by the incline. While the surface tension from the catechol solutions indicated no obvious trend among concentrations, it decreased when the riboflavin concentration increased from 10 μM to 1000 μM (Figure 3.5). In the context of Equation 2, at 10 μM of riboflavin solution for example, the smallest contact angle, which led to the largest value of its cosine, in addition to the largest surface tension resulted in the largest capillary pressure value (Figure 3.4, 3.5). At higher concentrations for riboflavin, this reducing capillarity pressure therefore enhanced the water saturation except for 1000 μM. A wider finger width at higher concentration except for 1000 μM might due to a decrease in water holding capacity, where water diffused more into the dry soil matrix. Moreover, by adding chemicals, the surface tension of water could decrease and therefore the fingers' size would reduce (Glass et al., 1989a). Although the phenomenon described by Glass et al. (1988) is opposite to our findings, the study above further supports that surface tension also plays a role in changing the preferential flow process.

Previous point source experiments have determined that at the same flow rate with a lower contact angle of media, the fingers tend to be more bulbous and wider than under a higher contact angle (Wallach et al., 2013). However, our observance of the

fingers from the catechol and riboflavin solutions indicated a decreased contact angle that narrowed the bulbous finger shapes with an increase in catechol concentration and a decrease in riboflavin concentration. The findings could have resulted because the infiltration process was conducted by simulating a random rain event rather than using point source dripping. The application of the random rain event completely saturated the top layer. Consequently, the capillary force acting on the wetting front that caused the finger to spread was slightly smaller as compared to the gravitational force. Therefore, for the lower contact angles, the bulbous shape failed to persevere as gravity caused the eventual elongation of all fingers to different degrees of shapes at the respective contact angles and surface tensions.

As finger flows through a porous medium, the water carries solutes and nutrients to microbes in pores, and in turn the microbes and their exudates also possibly affect the finger flow pattern and water distribution. As a degraded intermediate of aromatic compound, catechol is poisonous and possibly harmful to microbes. As the catechol concentration increases from 10 to 1000 μM, the fingers become narrower and produce more branches (Figure 3.9). A possible relationship between microbial behaviors and fingering flow may manifest the microbes metabolizing to more rapidly dispense with the catechol faster, as they increase the contact area to the surrounding matrix and minimize or narrow the internal hold zone for the catechol. An increased water saturation percentage at higher concentration may also be useful in catalyzing the chemical reactions in a wet system. However, riboflavin also serves as nutrient for microbes. Specifically, in studies with riboflavin at increased concentrations from 10 to 1000 μM,

the fingers were observed to grow wider except for the 1000 μM sample (Figure 3.11). A possible explanation is that the riboflavin exudate effect on the preferential flow is tied to the degree to which the microbes favor this nutrient. At higher concentrations of riboflavin solution (500 μM), microbes might favor this nutrient and wish to retain it for further use, which leads to wider fingers and a maximum internal zone. However, once the concentration reaches to 1000 μM, which might be too high for microbes, the flow pattern becomes narrow again. The highest water saturation percentage at 500 μM of concentration observed in profiles creates the wettest system for the maximum microbial activity.

This research so far has used the LTM to evaluate the concentration effects of artificial microbial exudates on infiltration process, which was not yet widely studied. The use of LTM, an optical imagery system using visible light, has been used in such diverse applications as contaminant hydrogeology, in the measurement of flow paths and in determining the velocity of both fluid and solutes, and in characterizing both fluid distribution and contaminant transport (Werth et al., 2010). Many such optical methods have been used to evaluate many biotic and abiotic systems in either saturated or unsaturated porous media. However, very little research has been undertaken on unsaturated systems, and only a few studies emphasizing the process of infiltration (Keller and Auset, 2007). Of the studies analyzing biomass growth, microbial and colloidal transport, and biofilm process in unsaturated porous media, most only involved the use of optical methods to qualitatively visualize pore-scale flow or transport, with additional results derived from a further model calculation or graphing breakthrough

curves (Auset et al., 2005; Dunsmore et al., 2004; Sirivithayapakorn and Keller, 2003). The application of LTM in this research directly related image information (i.e. light intensity) to flow characteristics (i.e. water saturation percentage) quantitatively through calibration greatly simplified the data acquisition process. The study also filled the gap and expanded the research regarding infiltration process related to microbial activity, where the previously mentioned study solely looked at the contact angle influence (Wallach et al., 2013). This paper, however, was more specific to types and concentrations of fluid. Infiltration, as one of the most important processes that occurs in natural systems is worth investigating given its effects on both biotic and abiotic characteristics in subsurface. Future research must entail the use of actual microbes and different biomass concentrations, which closely corresponds to the various microbial exudate concentrations. A departure from the analysis of microbial transport, biofilm growth or bioclogging would involve studying the effect of microbial existence on infiltration process in nearby flowing water.

Furthermore, the evolution of the research involving microbes should emphasize the secreted microbial exudates diffusing from those microbes, which may cause a change in the water gradient potential around the microbial colony. A study using the LTM to reveal the microbial exudates' distribution around living microbes and to evaluate the relationship between media moisture and exudates' diffusion process (e.g. rate) would be quite interesting. The integration of hysteresis with repeated wetting and drying cycles to investigate the influence of microbes and microbial exudates is also recommended. The image and data acquired from imaging techniques will be useful for

depicting colony morphology in porous media, to show the shifting variations in water content between dry and wet conditions, and to explain the water uptake strategies used by microbes under changing media hydrological properties (Carminati et al., 2016).

5. Conclusion

The important findings of this 2D tank microbial exudate flow study are summarized below:

- Microbial exudates affected the preferential flow during the infiltration process by forming two zones in the vertical water content profiles for both of the artificial exudate-added solutions, catechol and riboflavin, rather than three zones in the NaCl control solution. This formation is perhaps from the enhancement in the water retaining capacity of the porous medium.
- An examination of the infiltration process under the same intake flow rate determined the influence of various concentrations upon the preferential flow, which was indicated by different water content profiles.
- The interfacial measurements and distinguished flow patterns of the two microbial exudates indicated different actions of each upon the infiltration process.
- An increased wettability of the catechol solutions was caused by a reduced contact angle at higher concentrations, which created more branches in the fingers that greatly accelerated the time to saturation.
    - A faster finger moving velocity, a greater water saturation percentage, and a narrower finger width were observed at higher concentrations. An

increase in water holding capacity at higher concentration was hypothesized as the main cause of this phenomenon.

- The contact angle within the riboflavin solutions increased with a corresponding increase in concentration, which decreased the wettability at higher concentration.
    - A slower finger moving velocity, a small increase in water saturation percentage at the fingertip, and a larger width of the overall finger size was observed as the riboflavin concentration increased from 10 to 500 μM. The reduced capillarity gave a greater saturation at fingertip at higher concentration of riboflavin.
- Possible relationships between the microbial activity and preferential flow characteristics were assumed according to the properties of chemicals.
    - Microbes may try to minimize contact with catechol and tend to affect the preferential flow by narrowing the finger.
    - Microbes favor the usage of riboflavin and tend to increase the width of fingers.

6. Tables and Figures

Table 3.1 The characteristics of the main fingers for catechol and riboflavin solutions and the NaCl control solution

		Numbers of Fingers			Velocity of The Main Finger [cm/min]			Main finger length [cm]			Main finger width at 90% of length [cm]		
		Replicate 1	Replicate 2	Average	Replicate 1	Replicate 2	Average	Replicate 1	Replicate 2	Average	Replicate 1	Replicate 2	Average
Catechol	10µM	2	1	1.5	1.63	2.05	1.84	27.69	26.59	27.14	11.72	7.66	9.69
	100µM	2	2	2	1.76	1.82	1.79	28.23	27.23	27.73	6.11	7.23	6.67
	500µM	2	2	2	2.04	1.70	1.87	28.54	27.21	27.88	7.24	7.59	7.41
	1000µM	2	2	2	2.17	1.69	1.93	28.18	26.98	27.58	5.08	5.16	5.12
Riboflavin	10µM	2	2	2	2.07	1.47	1.77	26.94	23.55	25.25	6.66	7.25	6.96
	100µM	2	1	1.5	1.87	2.18	2.03	26.25	28.29	27.27	6.97	7.71	7.34
	500µM	2	3	2.5	1.88	1.74	1.81	28.24	27.92	28.08	9.84	4.88	7.36
	1000µM	2	2	2	1.63	1.48	1.55	27.71	28.09	27.90	7.16	8.33	7.75
NaCl	0.1 M	3	2	2.5	1.62	1.60	1.61	27.56	27.29	27.43	8.40	6.08	7.24

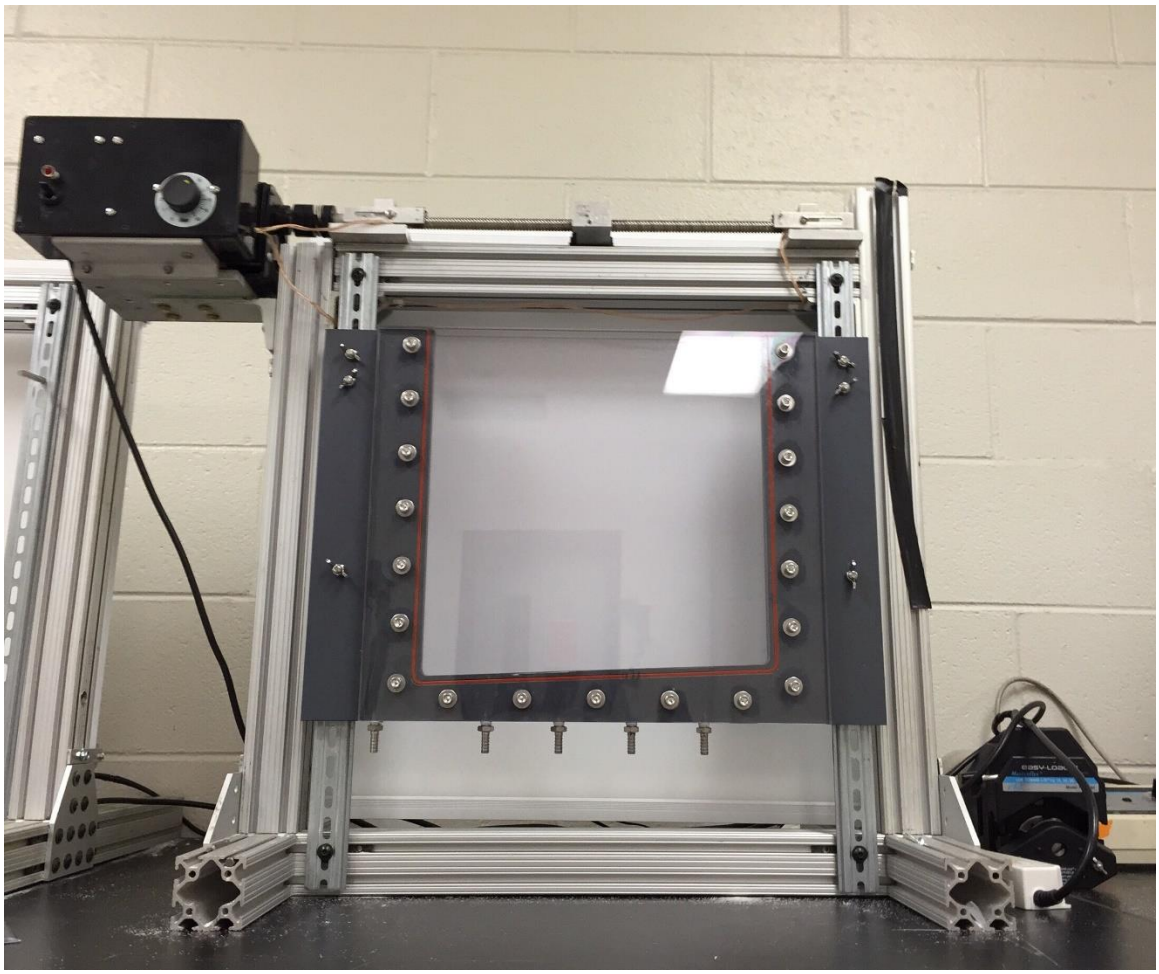

Figure 3.1 An overall structure and configuration of the 2D tank

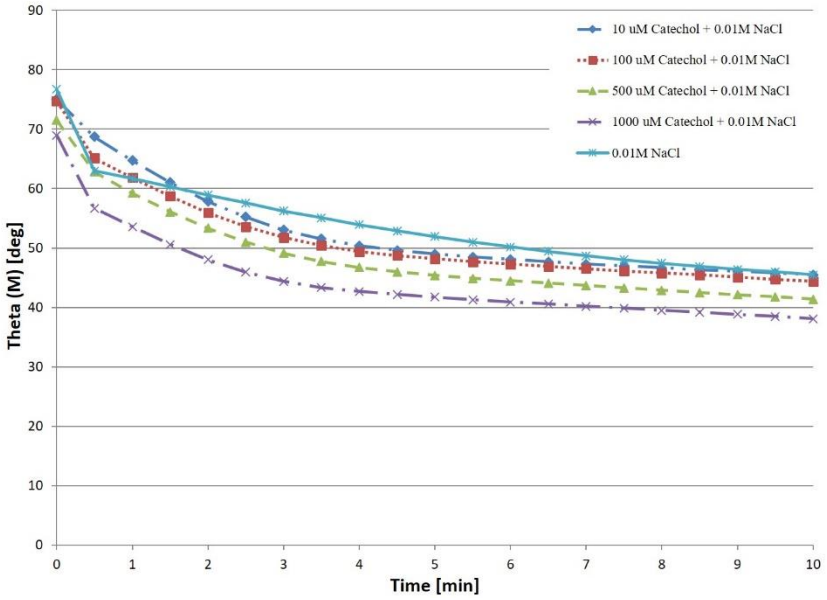

Figure 3.2 Contact angle measurements for the catechol solution at concentrations of 10, 100, 500, and 1000 μM

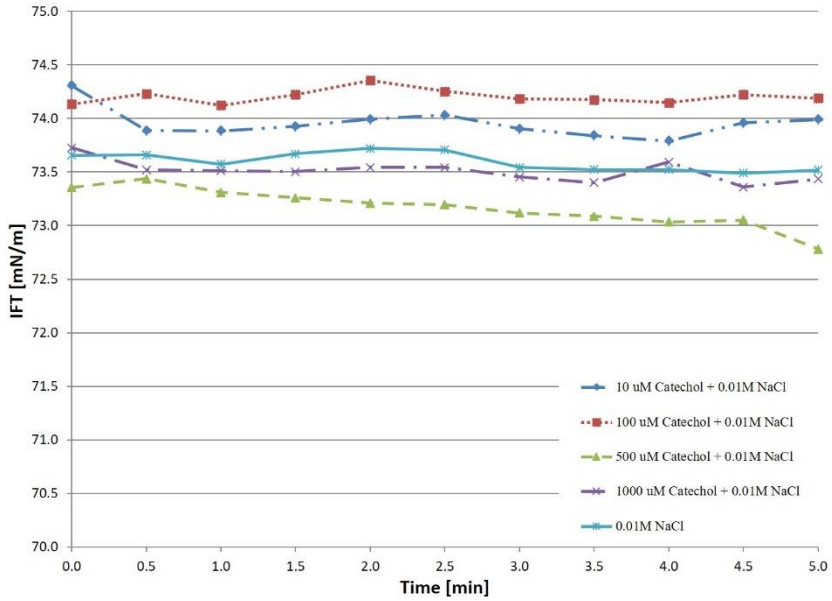

Figure 3.3 Surface tension measurements for the catechol solution at concentrations of 10, 100, 500, and 1000 μM

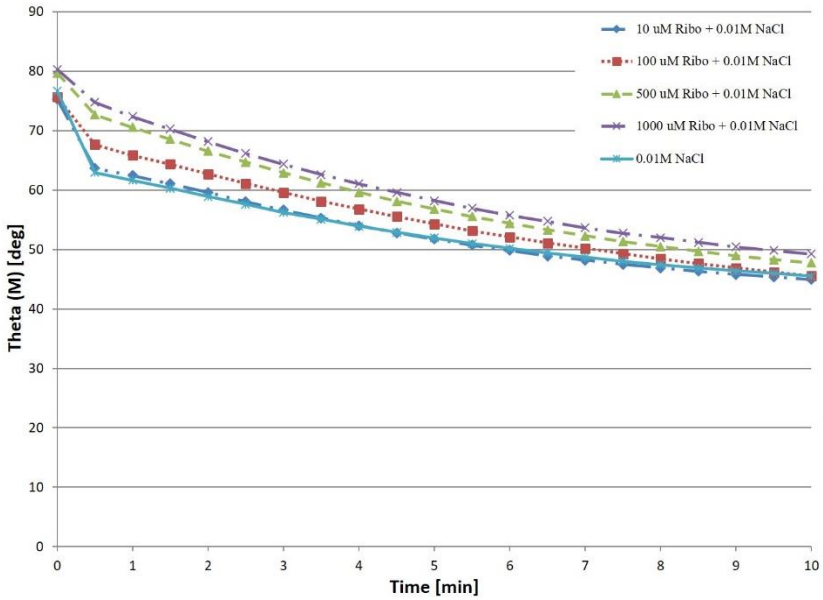

Figure 3.4 Contact angle measurements for the riboflavin solution at concentrations of 10, 100, 500, and 1000 μM

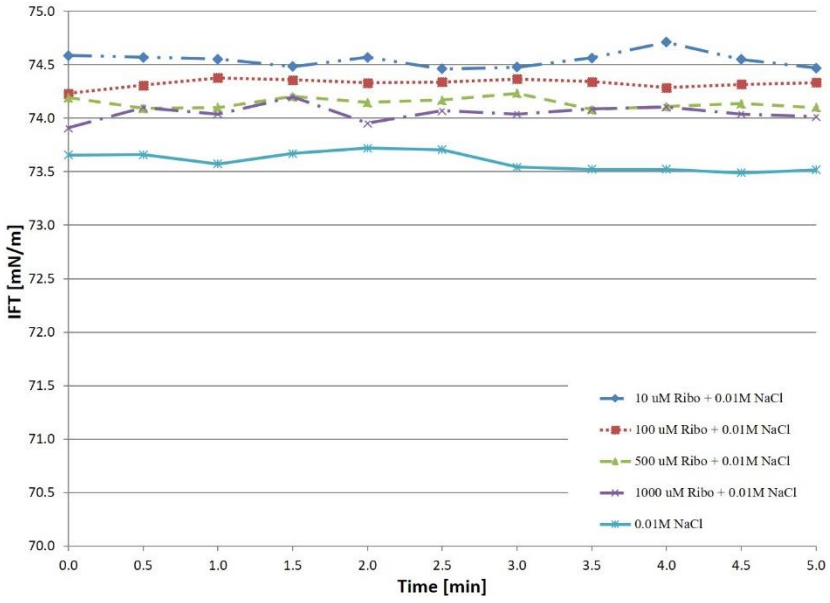

Figure 3.5 Surface tension measurements for the riboflavin solution at concentrations of 10, 100, 500, and 1000 μM

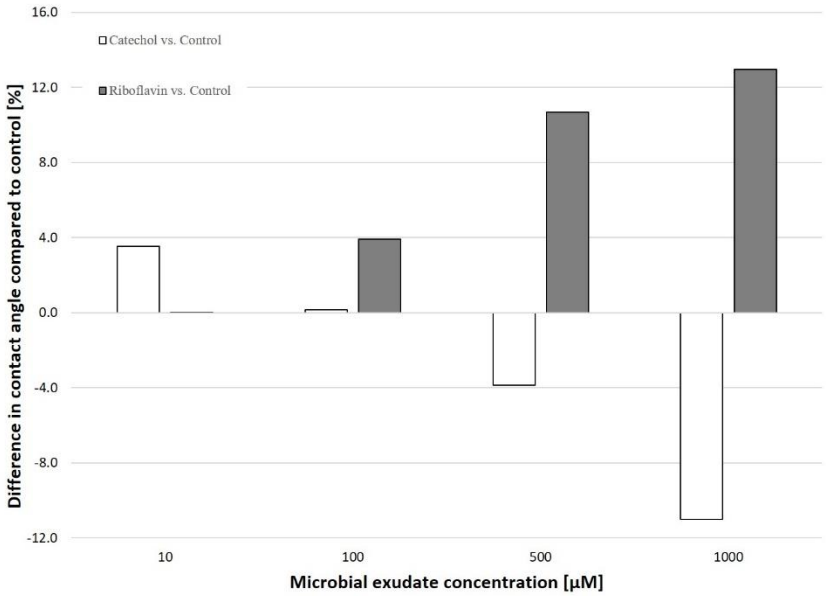

Figure 3.6 Percentage change of contact angle for microbial exudate solutions compared to NaCl control

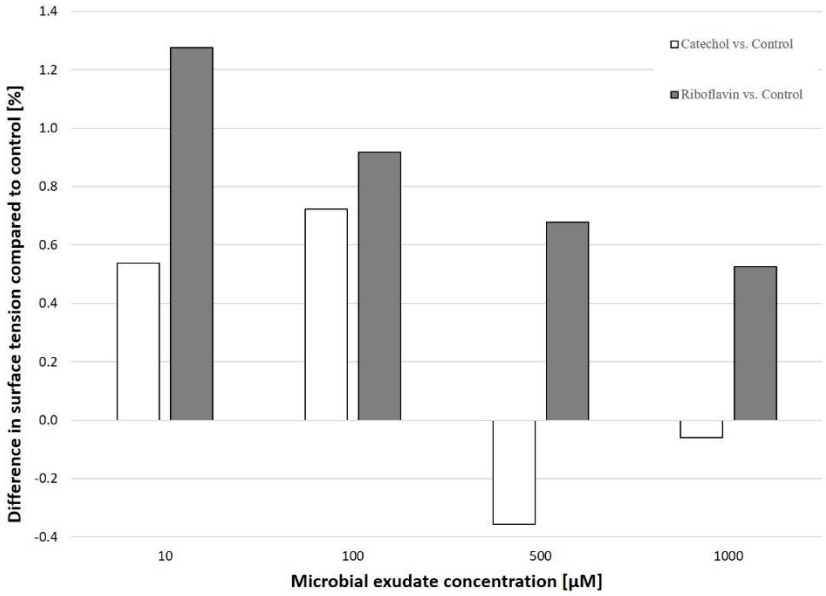

Figure 3.7 Percentage change of surface tension for microbial exudate solutions compared to NaCl control

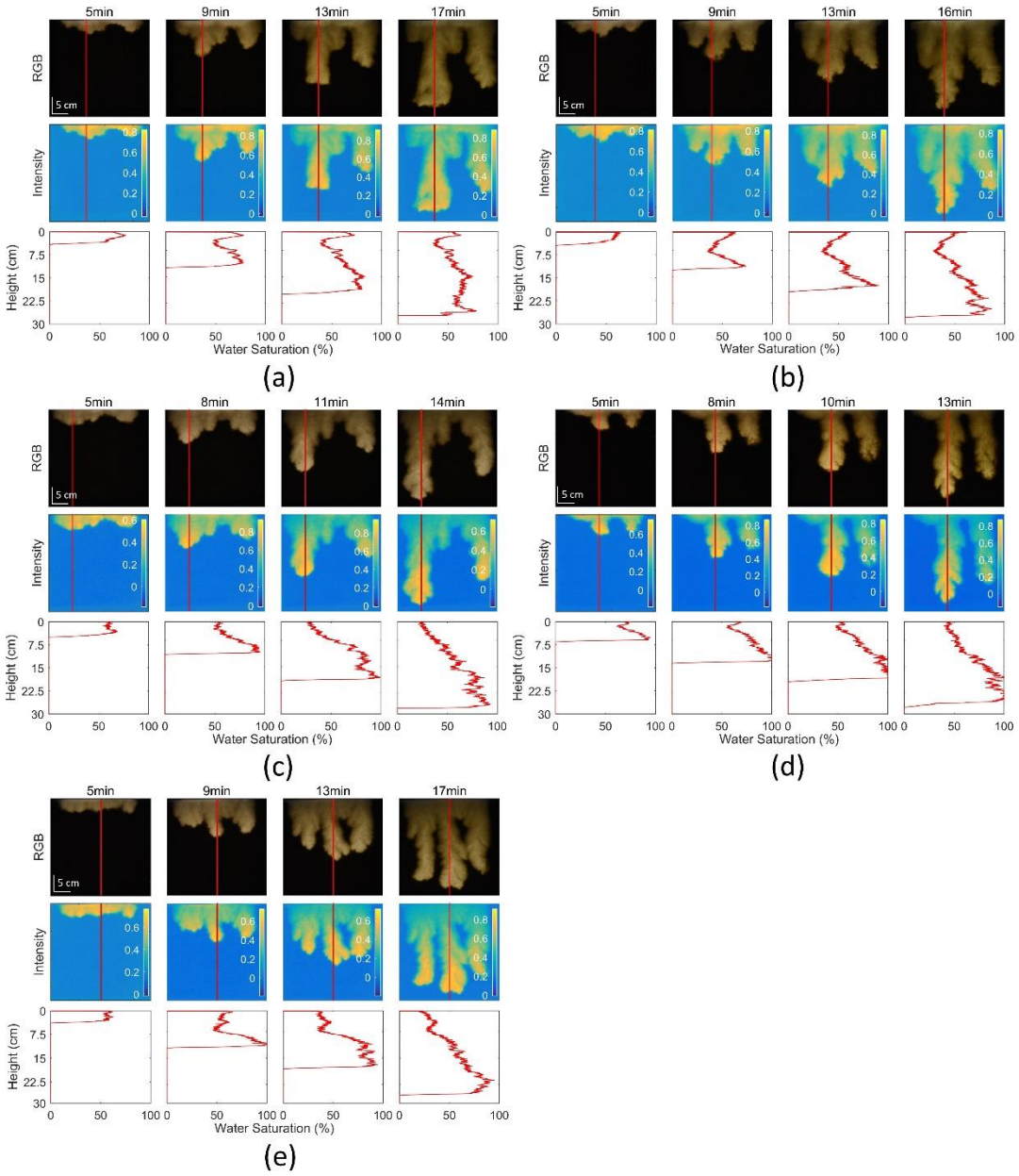

Figure 3.8 Vertical profile analysis for catechol solution at different stages of the main finger formation. Row 1 is the original RGB picture, Row 2 is the Matlab processed image with intensity only, Row 3 is the converted water saturation percentage distribution along the center of the main finger. (a) Concentration at 10 μM; (b) Concentration at 100 μM; (c) Concentration at 500 μM; (d) Concentration at 1000 μM; (e) NaCl control solution for comparison.

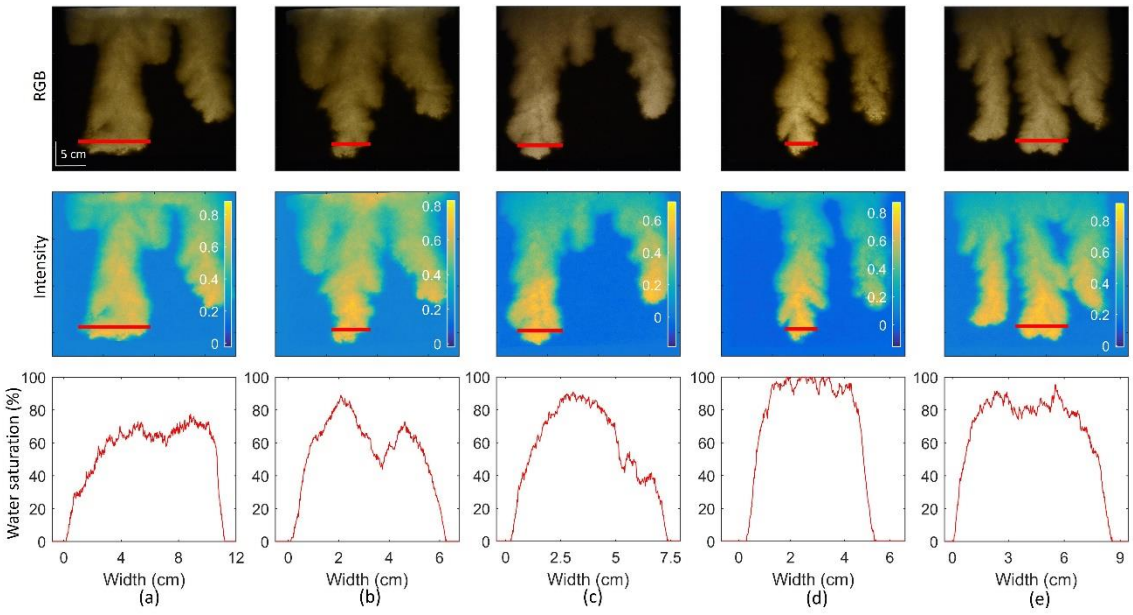

Figure 3.9 Horizontal profile analysis for catechol solution at the final stage of the main finger formation: (a) Concentration at 10 μM; (b) Concentration at 100 μM; (c) Concentration at 500 μM; (d) Concentration at 1000 μM; (e) NaCl control solution for comparison.

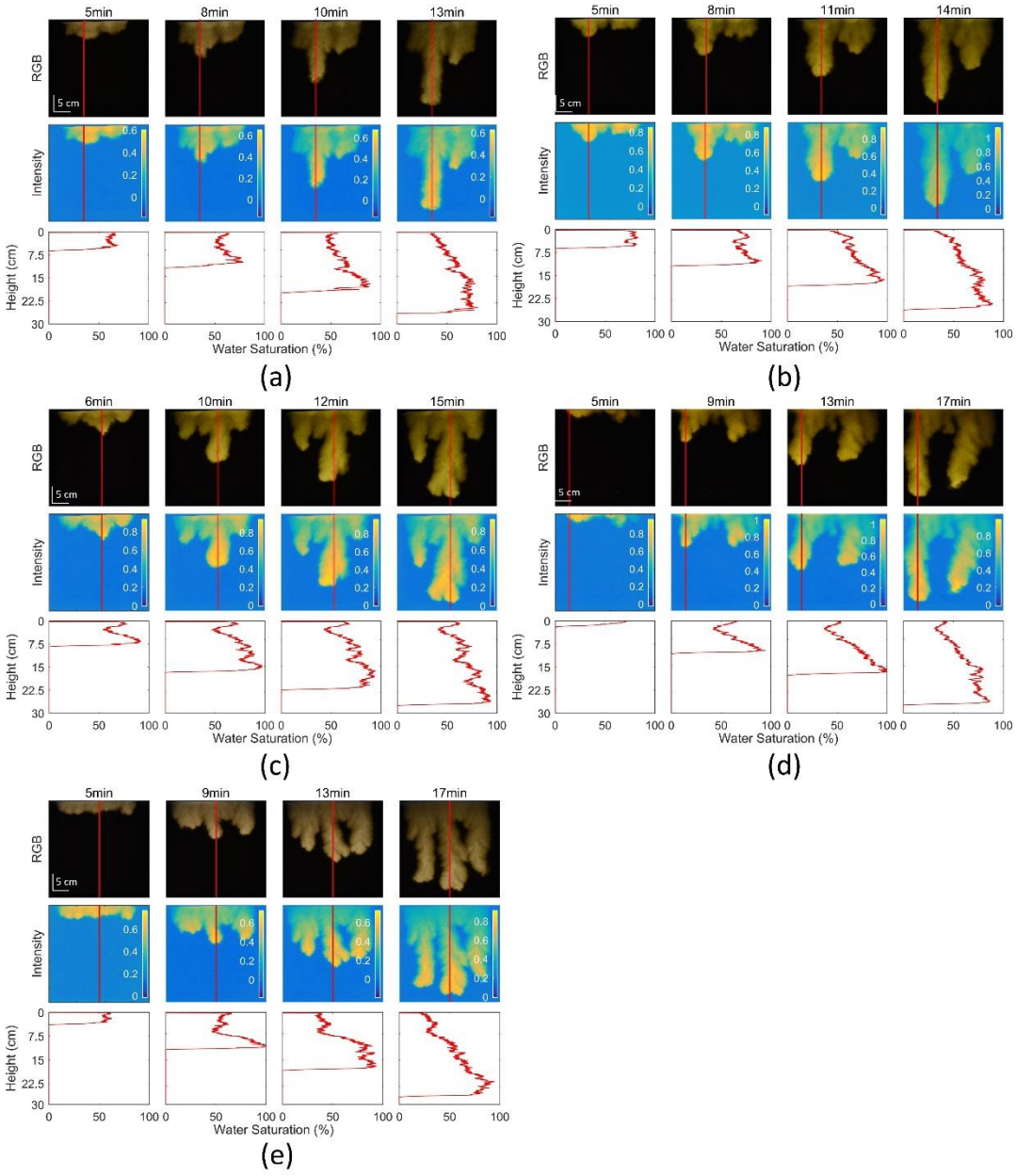

Figure 3.10 Vertical profile analysis for riboflavin solution at different stages of the main finger formation. Row 1 is the original RGB picture, Row 2 is the Matlab processed image with intensity only, Row 3 is the converted water saturation percentage distribution along the center of the main finger. (a) Concentration at 10 μM; (b) Concentration at 100 μM; (c) Concentration at 500 μM; (d) Concentration at 1000 μM; (e) NaCl control solution for comparison.

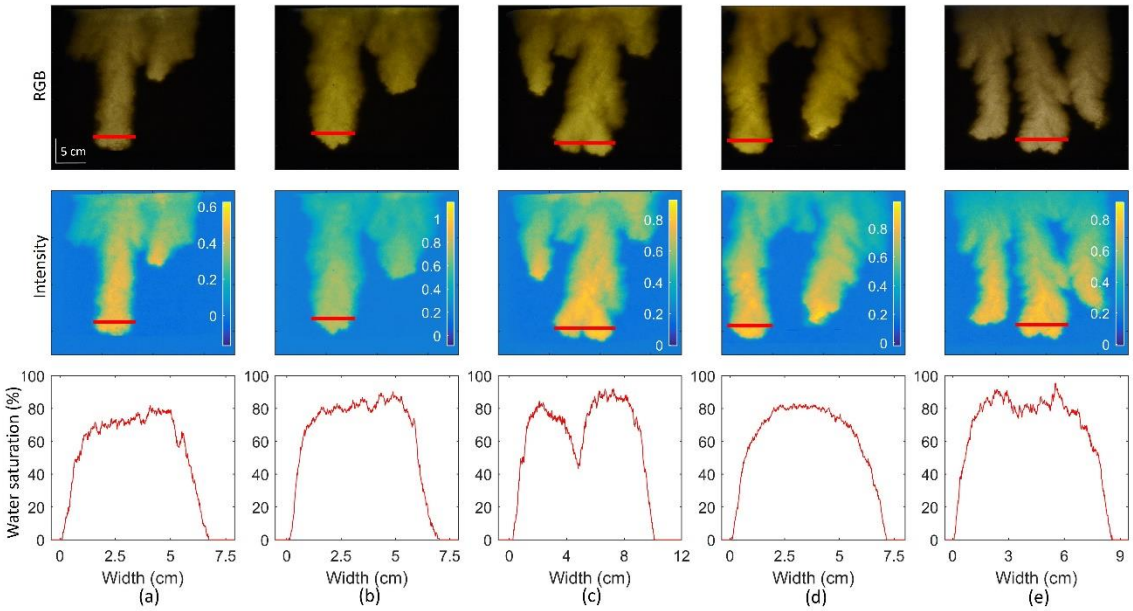

Figure 3.11 Horizontal profile analysis for riboflavin solution at the final stage of the main finger formation: (a) Concentration at 10 μM; (b) Concentration at 100 μM; (c) Concentration at 500 μM; (d) Concentration at 1000 μM; (e) NaCl control solution for comparison.

7. Acknowledgments

This material is based upon work supported by the U.S. Department of Energy Office of Science, Office of Basic Energy Sciences and Office of Biological and Environmental Research under Award Number DE-SC-00012530.

8. References

Andreini, M.S., Steenhuis, T.S., 1990. Preferential paths of flow under conventional and conservation tillage. Geoderma 46, 85–102. doi:10.1016/0016-7061(90)90009-X

Auset, M., Keller, A.A., Brissaud, F., Lazarova, V., 2005. Intermittent filtration of bacteria and colloids in porous media. Water Resour. Res. 41. doi:10.1029/2004WR003611

Bacher, A., Eberhardt, S., Eisenreich, W., Fischer, M., Herz, S., Illarionov, B., Kis, K., Richter, G., 2001. Biosynthesis of riboflavin. Vitam. Horm. 61, 1–49. doi:10.1016/S0083-6729(01)61001-X

Baker, R.S., Hillel, D., 1990. Laboratory tests of a theory of fingering during infiltration into layered soils. Soil Sci. Soc. Am. J. 54, 20–30.

Bashir, R., Smith, J.E., Henry, E.J., Stolle, D., 2009. On the importance of hysteresis in numerical modeling of surfactant-induced unsaturated flow. Soil Sediment Contam. 18, 264–283. doi:10.1080/15320380902772638

Bashir, R., Smith, J.E., Stolle, D.F., 2008. Surfactant-Induced Unsaturated Flow : Instrumented Horizontal Flow Experiment and Hysteretic Modeling. Soil Sci. Soc. Am. J. 72, 1510–1519. doi:10.2136/sssaj2007.0259

Bauters, T.W.., Steenhuis, T.., DiCarlo, D.., Nieber, J.., Dekker, L.., Ritsema, C.., Parlange, J.-Y., Haverkamp, R., 2000. Physics of water repellent soils. J. Hydrol. 231, 233–243. doi:10.1016/S0022-1694(00)00197-9

Baveye, P., Boast, C.W., Ogawa, S., Parlange, J.-Y., Steenhuis, T., 1998. Influence of image resolution and thresholding on the apparent mass fractal characteristics of preferential flow patterns in field soils. Water Resour. Res. 34, 2783–2796. doi:10.1029/98WR01209

Boot, C.M., Schaeffer, S.M., Schimel, J.P., 2013. Static osmolyte concentrations in microbial biomass during seasonal drought in a California grassland. Soil Biol. Biochem. 57, 356–361. doi:10.1016/j.soilbio.2012.09.005

Bras, R., 1990. Hydrology: an introduction to hydrologic science. Reading: Addison-Wesley, MA.

Carminati, A., Zarebanadkouki, M., Kroener, E., Ahmed, M.A., Holz, M., 2016. Biophysical rhizosphere processes affecting root water uptake. Ann. Bot. 118, 561–571. doi:10.1093/aob/mcw113

Celia, M.A., Bouloutas, E.T., Zarba, R.L., 1990. A general mass-conservative numerical solution for the unsaturated flow equation. Water Resour. Res. 26, 1483–1496. doi:10.1029/WR026i007p01483

Czarnes, S., Hallett, P.D., Bengough, a. G., Young, I.M., 2000. Root- and microbial-derived mucilages affect soil structure and water transport. Eur. J. Soil Sci. 51, 435–443. doi:10.1046/j.1365-2389.2000.00327.x

Darnault, C.J.G., DiCarlo, D.A., Bauters, T.W.J., Jacobson, A.R., Throop, J.A.,

Montemagno, C.D., Parlange, J.Y., Steenhuis, T.S., 2001. Measurement of fluid contents by light transmission in transient three-phase oil-water-air systems in sand. Water Resour. Res. 37, 1859–1868. doi:10.1029/2000WR900380

Darnault, C.J.G., Throop, J.A., DiCarlo, D.A., Rimmer, A., Steenhuis, T.S., Parlange, J.-Y., 1998. Visualization by light transmission of oil and water contents in transient two-phase flow fields. J. Contam. Hydrol. 31, 337–348. doi:10.1016/S0169-7722(97)00068-5

Dekker, L.W., Ritsema, C.J., 1996. Preferential Flow Paths in a Water Repellent Clay Soil with Grass Cover. Water Resour. Res. 32, 1239–1249. doi:10.1029/96WR00267

Diment, G.A., Watson, K.K., 1985. Stability Analysis of Water Movement in Unsaturated Porous Materials: 3. Experimental Studies. Water Resour. Res. 21, 979–984. doi:10.1029/WR021i007p00979

Doerr, S.H., Ritsema, C.J., Dekker, L.W., Scott, D.F., Carter, D., 2007. Water repellence of soils: new insights and emerging research needs. Hydrol. Process. 21, 2223–2228. doi:10.1002/hyp.6762

Doerr, S.H., Shakesby, R.A., Dekker, L.W., Ritsema, C.J., 2006. Occurrence, prediction and hydrological effects of water repellency amongst major soil and land-use types in a humid temperate climate. Eur. J. Soil Sci. 57, 741–754. doi:10.1111/j.1365-2389.2006.00818.x

Draths, K.M., Frost, J.W., 1995. Environmentally Compatible Synthesis of Catechol from D-Glucose. J. Am. Chem. Soc. 117, 2395–2400.

Du, X., Yao, T., Stone, W.D., Hendrickx, J.M.H., 2001. Stability analysis of the unsaturated water flow equation: 1. Mathematical derivation. Water Resour. Res. 37, 1869–1874. doi:10.1029/2001WR900004

Dunsmore, B.C., Bass, C.J., Lappin-Scott, H.M., 2004. A novel approach to investigate biofilm accumulation and bacterial transport in porous matrices. Environ. Microbiol. 6, 183–187. doi:10.1046/j.1462-2920.2003.00546.x

Ettema, C.H., Wardle, D.A., 2002. Spatial soil ecology. Trends Ecol. Evol. 17, 177–183. doi:10.1016/S0169-5347(02)02496-5

Glass, R.J., 1985. A study of wetting front instability in layered porous media. Cornell University, Ithaca, NY.

Glass, R.J., Cann, S., King, J., Baily, N., Parlange, J.-Y., Steenhuis, T.S., 1990. Wetting front instability in unsaturated porous media: A three-dimensional study in initially dry sand. Transp. Porous Media 5, 247–268. doi:10.1007/BF00140015

Glass, R.J., Parlange, J.-Y., Steenhuis, T.S., 1991. Immiscible Displacement in Porous Media: Stability Analysis of Three-Dimensional, Axisymmetric Disturbances With Application to Gravity-Driven Wetting Front Instability. Water Resour. Res. 27, 1947–1956. doi:10.1029/91WR00836

Glass, R.J., Parlange, J.-Y., Steenhuis, T.S., 1989a. Wetting front instability: 1. Theoretical discussion and dimensional analysis. Water Resour. Res. 25, 1187–1194.

Glass, R.J., Steenhuis, T.S., Parlange, J.-Y., 1989b. Wetting front instability: 2. Experimental determination of relationships between system parameters and two-

dimensional unstable flow field behavior in initially dry porous media. Water Resour. Res. 25, 1195–1207.

Glass, R.J., Steenhuis, T.S., Parlange, J.-Y., 1989c. Mechanism for finger persistence in homogeneous, unsaturated, porous media: Theory and verification. Soil Sci. 148, 60–70.

Gray, D., Norum, D., 1967. the Effect of Soil Moisture on Infiltration As Related To Runoff and Recharge. Proc. Hydrol. Symp. November, 133–153.

Green, H.W., Ampt, G.A., 1911. Studies on Soil Phyics. J. Agric. Sci. 4, 1–24. doi:10.1017/S0021859600001441

Griffin, D.M., 1981. Water and Microbial Stress, in: Alexander, M. (Ed.), Advances in Microbial Ecology. Springer US, Boston, MA, pp. 91–136. doi:10.1007/978-1-4615-8306-6_3

Halverson, L.J., Jones, T.M., Firestone, M.K., 2000. Release of intracellular solutes by four soil bacteria exposed to dilution stress. Soil Sci. Soc. Am. J. 64, 1630–1637.

Hendrickx, J.M.H., Flury, M., 2001. Uniform and preferential flow mechanisms in the vadose zone. Concept. Model. flow Transp. Fract. vadose Zo. Washington, DC 149–187. doi:doi:10.17226/10102

Henry, E.J., Smith, J.E., 2002. The effect of surface-active solutes on water flow and contaminant transport in variably saturated porous media with capillary fringe effects. J. Contam. Hydrol. 56, 247–270.

Hill, D.E., Parlange, J.-Y., 1972. Wetting front instability in layered soils. Soil Sci. Soc. Am. J. 36, 697–702.

Hillel, D., Baker, R.S., 1988. A descriptive theory of fingering during infiltration into layered soils. Soil Sci. 146, 51–56.

Hoa, N.T., 1981. A new method allowing the measurement of rapid variations of the water content in sandy porous media. Water Resour. Res. 17, 41–48. doi:10.1029/WR017i001p00041

Karagunduz, A., Young, M.H., Pennell, K.D., 2015. Influence of surfactants on unsaturated water flow and solute transport. Water Resour. Res. 51, 1977–1988. doi:10.1002/2014WR015845

Keller, A.A., Auset, M., 2007. A review of visualization techniques of biocolloid transport processes at the pore scale under saturated and unsaturated conditions. Adv. Water Resour. 30, 1392–1407. doi:10.1016/j.advwatres.2006.05.013

Kieft, T.L., soroker, E., firestone, M.K., 1987. Microbial biomass response to a rapid increase in water potential when dry soil is wetted. Soil Biol. Biochem. 19, 119–126. doi:10.1016/0038-0717(87)90070-8

Kim, Y.-J., Darnault, C.J.G., Bailey, N.O., Parlange, J., Steenhuis, T.S., 2005. Equation for describing solute transport in field soils with preferential flow paths. Soil Sci. Soc. Am. J. 69, 291–300. doi:10.1084/jem.20070109

Kostka, S.., 2000. Amelioration of water repellency in highly managed soils and the enhancement of turfgrass performance through the systematic application of surfactants. J. Hydrol. 231, 359–368. doi:10.1016/S0022-1694(00)00208-0

Li, W., Xie, D., Frost, J.W., 2005. Benzene-Free Synthesis of Catechol : Interfacing Microbial and Chemical Catalysis. J. Am. Chem. Soc. 127, 2874–2882.

Lord, D.L., Demond, A.H., Salehzadeh, A., Hayes, K.I.M.F., 1997. Influence of Organic Acid Solution Chemistry on Subsurface Transport. 2. Capillary Pressure - Saturation. Environ. Sci. Technol. 31, 2052–2058.

Morales, V.L., Parlange, J.-Y., Steenhuis, T.S., 2010. Are preferential flow paths perpetuated by microbial activity in the soil matrix? A review. J. Hydrol. 393, 29–36. doi:10.1016/j.jhydrol.2009.12.048

Nair, C.I., Jayachandran, K., Shashidhar, S., 2008. Biodegradation of phenol. African J. Biotechnol. 7, 4951–4958.

Parlange, J.Y., Hill, D.E., 1976. Theoretical analysis of wetting front instability in soils. Soil Sci. 122, 236–239.

Passioura, J.B., 1988. Water Transport in and to Roots. Annu. Rev. Plant Physiol. Plant Mol. Biol. 39, 245–265. doi:10.1146/annurev.pp.39.060188.001333

Perkins, J.B., Pero, J.G., 1993. Bacillus subtilis and Other Gram-Positive Bacteria: Biosynthesis of riboflavin, biotin, folic acid, and cobalamin., American Society of Microbiology.

Perkins, J.B., Sloma, A., Hermann, T., Theriault, K., Zachgo, E., Erdenberger, T., Hannett, N., Chatterjee, N., Williams II, V., Rufo Jr, G., Hatch, R., Pero, J., 1999. Genetic engineering of Bacillus subtilis for the commercial production of riboflavin. J. Ind. Microbiol. Biotechnol. 22, 8–18.

Philip, J.R., 1975a. Stability analysis of infiltration. Soil Sci. Soc. Am. J. 39, 1042–1049.

Philip, J.R., 1975b. The growth of disturbances in unstable infiltration flows. Soil Sci. Soc. Am. J. 39, 1049–1053.

Potts, M., 1994. Desiccation tolerance of prokaryotes. Microbiol. Mol. Biol. Rev. 58, 755–805.

Raats, P.A.C., 1973. Unstable wetting fronts in uniform and nonuniform soils. Soil Sci. Soc. Am. J. 37, 681–685.

Read, D.B., Bengough, A.G., Gregory, P.J., Crawford, J.W., Robinson, D., Scrimgeour, C.M., Young, I.M., Zhang, K., Zhang, X., 2003. Plant roots release phospholipid surfactants that modify the physical and chemical properties of soil. New Phytol. 157, 315–326. doi:10.1046/j.1469-8137.2003.00665.x

Read, D.B., Gregory, P.J., 1997. Surface tension and viscosity of axenic maize and lupin root mucilages. New Phytol. 137, 623–628. doi:10.1046/j.1469-8137.1997.00859.x

Schallmey, M., Singh, A., Ward, O.P., 2004. Developments in the use of Bacillus species for industrial production. Can. J. Microbiol. 50, 1–17. doi:10.1139/W03-076

Selker, J.S., Steenhuis, T.S., Parlange, 1992. Wetting front instability in homogeneous sandy soils under continuous infiltration. Soil Sci. Soc. Am. J. 56, 1346–1350.

Sirivithayapakorn, S., Keller, A., 2003. Transport of colloids in unsaturated porous media: A pore-scale observation of processes during the dissolution of air-water interface. Water Resour. Res. 39. doi:10.1029/2003WR002487

Smith, R.E., Corradini, C., Melone, F., 1993. Modeling infiltration for multistorm runoff events. Water Resour. Res. 29, 133–144. doi:10.1029/92WR02093

Stahmann, K.-P., Revuelta, J.L., Seulberger, H., 2000. Three biotechnical processes using Ashbya gossypii, Candida famata, or Bacillus subtilis compete with chemical riboflavin production. Appl. Microbiol. Biotechnol. 53, 509–516.

doi:10.1007/s002530051649

Steenhuis, T., Boll, J., Shalit, G., Selker, J., Merwin, I., 1994. A simple equation for predicting preferential flow solute concentrations. J. Environ. Qual. 23, 1058–1064.

Tamai, N., Asaeda, T., Jeevaraj, C.G., 1987. Fingering in two-dimensional, homogeneous, unsaturated porous media. Soil Sci. 144, 107–112.

Thakur, K., Tomar, S.K., De, S., 2016. Lactic acid bacteria as a cell factory for riboflavin production. Microb. Biotechnol. 9, 441–451. doi:10.1111/1751-7915.12335

Waechter, R.T., Philip, J.R., 1985. Steady Two- and Three-Dimensional Flows in Unsaturated Soil: The Scattering Analog. Water Resour. Res. 21, 1875–1887. doi:10.1029/WR021i012p01875

Wallach, R., Margolis, M., Graber, E.R., 2013. The role of contact angle on unstable flow formation during infiltration and drainage in wettable porous media. Water Resour. Res. 49, 6508–6521. doi:10.1002/wrcr.20522

Wang, L., Manzoni, S., Ravi, S., Riveros-Iregui, D., Caylor, K., 2015. Dynamic interactions of ecohydrological and biogeochemical processes in water-limited systems. Ecosphere 6, 1–27.

Wang, Z., Wu, Q.., Wu, L., Ritsema, C.., Dekker, L.., Feyen, J., 2000. Effects of soil water repellency on infiltration rate and flow instability. J. Hydrol. 231, 265–276. doi:10.1016/S0022-1694(00)00200-6

Werth, C.J., Zhang, C., Brusseau, M.L., Oostrom, M., Baumann, T., 2010. A review of non-invasive imaging methods and applications in contaminant hydrogeology research. J. Contam. Hydrol. 113, 1–24. doi:10.1016/j.jconhyd.2010.01.001

Yao, T., Hendrickx, J.M., 1996. Stability of wetting fronts in dry homogeneous soils under low infiltration rates. Soil Sci. Soc. Am. J. 60, 20–28.

Yao, T., Hendrickx, J.M.H., 2001. Stability analysis of the unsaturated water flow equation: 2. Experimental verification. Water Resour. Res. 37, 1875–1881. doi:10.1029/2001WR900003

Yuan, Y., Lee, T.R., 2013. Contact Angle and Wetting Properties, in: Bracco, G., Holst, B. (Eds.), Surface Science Techniques. Springer Berlin Heidelberg, Berlin, Heidelberg, pp. 3–34. doi:10.1007/978-3-642-34243-1_1

CHAPTER FOUR

APPLICATION OF OPTICAL IMAGING TECHNIQUE USING SENSING FOILS FOR DETECTION OF PH AND DISSOLVED O_2 CONCENTRATION DYNAMICS IN POROUS MEDIA

1. Introduction

Contamination in soil and water system from human activities due to industrialization and urbanization has brought a series adverse effect on environment and human health (Fu et al., 2014). According to the US Environmental Protection Agency's (EPA) record, heavy metals including Cd, Pb, Hg, Cu, Ni and Zn are considered as major contaminants in environment (Cameron, 1992). Pollutants contained in municipal and industrial effluents are released into environment if they are not treated thoroughly in wastewater treatment plants, and will adsorb and deposit in soil and leach to water bodies or even groundwater systems. Potential uptake and bioaccumulation of those contaminants are hazardous when exposed to living organisms (Blossfeld et al., 2010; Christensen, 1984; Mulligan et al., 2001).

In order to remediate and remove the contaminants in environment, various technologies and materials are developed and used. As one of the common remediation approaches, immobilization is important and beneficial when treating heavy metals (Wuana and Okieimen, 2011). Heavy metals tend to adsorb on soil particles once they are in the field, and then transform to other forms with varying mobility and toxicity through chemical and physical speciation (Buekers, 2007; Dube et al., 2001; Kot and Namiesńik, 2000; Levy et al., 1992; Wuana and Okieimen, 2011). The transport of heavy metals in the soil could be problematic if the metals leach to groundwater system, which will cause

further contamination (Dube et al., 2001; Kanungo and Mohapatra, 2000). Many physical and chemical characteristics of soil have shown to influence on metal speciation, its solubility and mobility, including soil pH, redox potential (Eh), temperature and organic matter content (Chuan et al., 1996; Dube et al., 2001; Mulligan et al., 2001; Sun et al., 2007). For example, studies have shown that metal pollutants are usually more mobilized in an acidic environment (Calmano et al., 1993; Dube et al., 2001). Unlike the general trend for pH effect, the mobility of metals after redox reactions varies based on types of metals and microenvironments (Violante et al., 2010).

Given that the condition of pH and redox potential is important on contaminant sites during remediation, two treatment techniques under related cases are chosen to discuss. In the case of acid mine drainage (AMD) treatment, the generated low pH effluents, for instance sulfuric acid from oxidation of FeS_2 from sulfide-bearing mines, can be mitigated by neutralization through adding limestone (Akcil and Koldas, 2006). In some treatments of AMD effluents, an application of passive approach using anoxic limestone drains (ALD) can add alkalinity to the drainage water and improve water quality when coupled with constructed wetlands (Johnson and Hallberg, 2005; Kleinmann et al., 1998). Zero valent iron (ZVI), on the other hand, is also treated as a remediation material by reacting with contaminants like metal oxides and organic compounds (Rangsivek and Jekel, 2005). When ZVI transfers electrons to oxidized metals, it reduces the contaminants to non- or less toxic forms of metals. During the reaction between ZVI and dissolved oxygen (DO), hydrogen peroxide (H_2O_2) is produced, which can further trigger oxidized Fe^{2+} to react with it to produce hydroxyl

radicals (•OH). The formation of this strong oxidizing agent targets on a broad range of organic pollutants and degrades them (Fu et al., 2014). A novel technique constructing a permeable reactive barrier (PRB) to treat groundwater is developed. The targeted contaminants could be inorganic, organic or radioactive depending on the usage of reactive materials in the PRB (Cundy et al., 2008). Some possible mechanisms for a ZVI-based PRB system to remove metals and radionuclides are through reductive precipitation, adsorption or complexation (Morrison et al., 2002; Scherer et al., 2000).

As mentioned previously, the pH and oxygen level (or redox potential) not only affect the mobility and transport of pollutants on contaminant sites, but also play an important role in soil living organisms and plants activities. Both pH value and oxygen concentration are heterogeneously distributed in soil systems (Brune et al., 2000; Fischer et al., 1989; Hinsinger et al., 2009, 2005; Jaillard et al., 1996). Knowing of their gradients or changes by locations will provide useful information about microbial community (Klimant et al., 1995) and plant (Rudolph et al., 2012) activity, and soil condition. In order to measure the changes in value of pH and dissolved oxygen, many different techniques and instruments have been developed from the traditional destructive approaches to nowadays non-invasive methods (Gregory and Hinsinger, 1999). Different from the use of arrays of microelectrodes (Schaller and Fischer, 1985), pH dye indicators developed by Weisenseel et al. (1979) were able to spatially measure the pH changes around the rhizosphere qualitatively. An innovation by coupling pH dye indicator with image analysis captured by camera has greatly improved the precision of measurement and resolution both in space and time (Gregory and Hinsinger, 1999; Jaillard et al., 1996).

Similarly, two traditional approaches to measure dissolved oxygen, which are Winkler method and the amperometric detector method, are less attractive compared to the novel developed optical oxygen sensors in microenvironment. The latter technique can quickly measure DO with a small amount of solution without stirring and consuming oxygen (McEvoy et al., 1996).

Applications of optical sensors in fields of plant, microbial and marine have increased rapidly in the last twenty years (Blossfeld and Gansert, 2007; Glud et al., 1998, 1996; Precht et al., 2004). There are many types of optical sensors developed to measure various physical and chemical parameters, including pH, DO, CO_2, and temperature (Fuller et al., 2003). The optical sensors, in this study specifically for fluorescence-based sensors, have shown considerable advantages. Besides the non-destructive measurement, those sensors are sensitive and reversible with a quick response time, and they also provide high spatial and temporal resolution of information acquired from the camera imaging (Baleizão et al., 2008; Rudolph et al., 2012). Possible limitations of optical sensors can come from camera drift and non-uniform lighting source (Borisov et al., 2006; Liebsch et al., 2000). General compositions of optical sensors contain fluorescent dyes bedded into polymeric matrix, and the final product looks like a thin sheet of foil. Depending on the type of dye and polymeric matrix selected, the fluorescence emitted by the dye changes when reacting with the tested parameters after excited by the light source (Rudolph et al., 2015). The emitted incident light is then captured and recorded by charge-coupled device (CCD) cameras and analyzed by software (Werth et al., 2010).

Up to date, numerous applications of fluorescence-based optical sensors are related to rhizosphere, biofilms and marine sediments (Glud et al., 1998; Precht et al., 2004; Rudolph et al., 2015, 2012). However, a few literatures study about the application of those sensors in scenario of contaminant remediation in soil or groundwater, where pH and dissolved oxygen greatly impact on pollutants' mobility and toxicity (e.g. Huang et al., 2003). This research focused on the measurement of pH and oxygen using optical sensor foils in a two-dimensional (2D) tank system. Simplified cases on contaminated sites, where only $CaCO_3$ and zero valent iron (ZVI) were added to sand media, were simulated for each sensor foil application test. Gradients of pH and oxygen were generated and monitored throughout the experiments. The goals of the study were mainly to evaluate the performance of pH and oxygen optical sensor foils in a 2D system under a simplified remediation environment, and the precision of measurement by checking the influents, effluents, and sampled solutions along the 2D tank during experiments.

2. Material & Methods

2.1. Optical imaging: principle and material preparation

2.1.1. pH optical sensor

The pH optical sensor works based on the selection of proton-permeable polymeric matrix. Its degree of protonation changes with respective pH value in the bulk solution, that is reflected by the emitted fluorescence spectra's intensity (Schröder et al., 2007; Weidgans et al., 2004). A normalized relationship between pH and fluorescence

intensity can be expressed by the Boltzmann equation shown in Equation 1, and the plot is in sigmoidal shape.

$$\frac{F}{F_0} = \frac{A_1 - A_2}{1+\exp(\frac{pH-pKa'}{p})} + A_2 \quad (1)$$

where F_0 is the fluorescence intensity captured at the highest pH chosen for calibration, F is the fluorescence intensity during experiment at other pH values, A_1 and A_2 are initial and final values determined by empirical factors, pKa' is the point of inflection, and p is the width of the sigmoidal plot (Rudolph et al., 2015; Schröder et al., 2007).

During preparation step for pH sensor foil, 9 g of ethanol and water mixture in a 9:1 ratio was prepared and used to dissolve 1 g of hydrogel (HydroMed D4, AdvanSource Biomaterials, Wilmington, MA). The produced 10% (w/w) of mixture solution was the stock for making polymeric matrix. For the pH sensing part, 10 mg of pH indicator 5-hexadecanoylaminofluorescein (HAF) (Thermo Fisher Scientific, USA) was prepared and mixed with 1 g of hydrogel. The two components were then stirred together for at least 12 hours, and later coated onto a 75 μm-thick transparent polyester sheet using a coating rod. The foil with the solvent air dried to a thickness of 10 μm at the ambient temperature and was stored in dark for later use (Rudolph et al., 2015).

2.1.2. Oxygen optical sensor

The mechanism for oxygen optical sensor relies on the fluorescence quenching effect of oxygen, where quantum yield of the sensor dye decreases when reacting with oxygen (Carraway et al., 1991a). Under the same temperature, the performance of quenching can be expressed in forms of Stern-Volmer equations shown in Equation 2.

$$\frac{\tau_0}{\tau} = 1 + K_{SV}[Q] \quad (2a)$$

$$K_{SV} = k_2\tau_0 \quad (2b)$$

$$\frac{I_0}{I} = 1 + \left(K_{SV} + K_{eq}\right)[Q] + K_{eq}K_{SV}[Q]^2 \quad (2c)$$

where τ_0 is the lifetime for sensor material when quencher is absent, τ is the lifetime under certain quencher concentration, I_0 is the fluorescence intensity when quencher is absent, I is the fluorescence intensity measured at certain quencher concentration, K_{SV} and k_2 are the Stern-Volmer and bimolecular quenching constants, K_{eq} is the associated constant from the binding of quencher and fluorescent species, and [Q] is the concentration of quencher, in this case oxygen (Carraway et al., 1991a, 1991b).

When preparing for the oxygen optical sensor, 20 mg of platinum (II) 5,10,15,20-tetrakis (2,3,4,5,6-pentafluorophenyl) porphyrin (PtTFPP) (Porphyrin systems, Germany) and 1.98 g of polystyrene were dissolved in 18 g of toluene (Sigma-Aldrich, St. Louis, MO) to create a "cocktail". The rest of the procedures for stirring and coating were similar with the ones for pH sensor preparation. The final product of oxygen foil had a thickness about 10 μm and were kept in dark for later use (Rudolph et al., 2015, 2012).

2.2. Calibration tests

2.2.1. pH optical sensor calibration

For pH optical sensor's calibration, the pH foil was cut into rectangles and fitted into cuvettes. The side with sensing material faced to the bulk surrounding, and the other side was fixed to touch the wall. The cuvettes were then filled with ASTM C778 Graded sand (U.S. Silica Company, Ottawa, IL), which was consistent with the application experiments. Nine buffer solutions from pH 3 to pH 7 with an increment of 0.5, which

were made from sodium phosphate dibasic dodecahydrate (Sigma-Aldrich, St. Louis, MO) and citric acid monohydrate (Sigma-Aldrich, St. Louis, MO) in proportions, were later injected into cuvettes in sequence to initiate the reactions. A blue LED array (Banner Engineering, Co, USA) with an excitation wavelength at 480 nm was chosen to be the light source. The LED light was anchored vertically towards the cuvettes, and a D5500 DSLR camera (Nikon, Tokyo, Japan) on a VTSL7200 72" tripod (Bower, Long Island City, NY) was positioned facing the setting. For all experiments in this study, an OD 2 long-pass 525 nm filter was put in front of the camera lens when taking images. Photos were continuously taken for two hours in order to monitor the time effect on the foils. The position for the camera, light and cuvettes were kept at the same place throughout the experiments (Figure 4.1).

2.2.2. Oxygen optical sensor calibration

Seven oxygen concentrations were simulated for O_2 sensor foil calibration test. Cuvettes were inserted with oxygen foils and filled with sand. When preparing for various DO-contained solutions, seven 160 mL of serum bottles were firstly purged with N_2 gas, and were poured with 60 mL of degassed ultrapure deionized (DI) water with a resistivity of 18.2 MΩ•cm (Millipore Corporation, Billerica, MA). Those bottles were then injected with 0, 5, 10, 20, 30, 40 and 50 mL of pure O_2 after taking out same volumes of N_2 using syringe to remain the same pressure inside. The bottles were sealed and left for overnight upside down. After reaching the gas-liquid equilibrium, the gases in headspace were sampled and tested by a gas chromatography to get a linear regression line, so that this process confirmed the accuracy of operations which would provide

credible DO concentrations later. The liquids with respective DO concentrations were extracted from the serum bottles and injected into the cuvettes in sequence. A UV LED light (Banner Engineering, Co, USA) with a wavelength of 395 nm was used to excite the foils, and pictures were taken by the DSLR camera continuously for two hours once the foils and solutions contacted. The concentrations of dissolved O_2 in water in unit of mg/L were later calculated based on Henry's law. The position for the camera, light and cuvettes were kept consistently throughout the experiments.

2.3. Applications in two-dimensional porous media system

2.3.1. Limestone neutralization with pH gradient

A two-dimensional (2D) tank with two plates made of scratch-resistant polycarbonate and an inner dimension of 30 cm × 1.2 cm × 30 cm (L×W×H) was used during the application experiments. Twelve evenly distributed sample pores were drilled on the back of the plate to withdraw solution if applicable for checking purpose. A simplified scenario for treatment of acid mine drainage was simulated, and sulfuric acid (Fisher Scientific, Waltham, MA) was prepared as the acid drainage solution. Bulk limestone containing mainly $CaCO_3$ (Sigma-Aldrich, St. Louis, MO) was crushed using a portable rock crusher (Sore Thumb, eBay), and sieved through a handmade 0.635 cm x 0.635 cm sifter modified from a piece of wire netting. The packing in 2D tank consisted of three layers. The top and bottom layers with a same depth of 7.5 cm applied just sand that was used during calibration, and the middle layer with a depth of 15 cm was filled with sand and $CaCO_3$ mixture with a mass ratio of 10:1. A long strip of foil was inserted into the center of the 2D tank that was later uniformly packed with media material.

During the experiment, a peristaltic pump head with a constant flow rate at 5 mL/min was used to pump acid solution into the tank. The end of the tube was positioned right above the midpoint of the tank and dripped solution as a point source. The blue LED light was on when all the other lights shut off, and pictures were taken continuously throughout the two-hour period. Besides the imaging taking, influent and effluents were gathered and checked using a pH meter.

2.3.2. ZVI barrier with dissolved oxygen gradient

By borrowing the ideas from contaminant treatment using ZVI and the reaction between ZVI and oxygen, a simplified context with ZVI applied was simulated in the 2D tank. A 1L stock of DI water was air bubbled for an hour and capped when not using. The packing for oxygen foil experiment also had three layers with the top and bottom layers filled with sand. The middle layer was a mixture of sand and ZVI (Sigma-Aldrich, St. Louis, MO) with a ZVI-to-sand mass ratio of 1:10. Other procedures including packing and pumping were similar with the pH ones. Images were taken continuously for two hours when the UV LED light was on. Influent and effluents were checked using the GC.

3. Results

3.1. pH optical sensor foil

Calibration curves for pH foil from pH of 3 to 7 were plotted against intensity values at 10min, 30min, 1hr and 2hr periods (Figure 4.2). The 4^{th} order polynomial trendline was used to express the calibration curves. When pH increased from 3 to 7, the intensity values became bigger except at the range from 6.5 to 7, where the intensity at

pH 7 was similar or even slightly smaller than that at 6.5. The four curves indicated that the time effect during the two-hour period was not significant overall and only slightly affected more at higher pH range from 6 to 7.

During the 2D tank experiment with crushed $CaCO_3$ applied, the strip of pH foil was analyzed using Matlab at 10min, 30min, 1hr and 2hr periods. The original RGB pictures were extracted to intensity figures, and a rectangle in the middle along the foil was selected to show vertical intensity profiles for later pH calculation purpose (Figure 4.3). At 10min, the acid solution did not yet fully flow through the mixture layer that left the bottom part darker. When time increased from 30min to 2hr, intensity maps became less intense and started to have more obvious winding flow marks on the right side. The intensity values along the vertical rectangle were then converted to pH values based on the calibration equations at respective time periods. The plots of pH values against vertical pixels at different time periods were shown in Figure 4.4. Gradients of pH were observed at top half of the foil which increased along the depth, whereas the pH values became similar at the bottom part. When time increased from 10min to 2hr, the pH profiles shifted from about 6.5 to 5. At bottom part of the foil, the pH profiles at 1hr and 2hr overlapped and did not show much difference.

3.2. Oxygen optical sensor foil

Calibration curves for oxygen foil from dissolved oxygen concentration of 0 to 20.74 mg/L were plotted against intensity values at 10min, 30min, 1hr and 2hr periods (Figure 4.5). The 2^{nd} order polynomial trendline was selected to express the calibration curves, and the shapes slightly curved upward. When DO concentrations increased, the

intensity values decreased respectively. After comparing the four calibration curves among two-hour period, the result indicated that the intensity values decreased when time length increased, and the time effect became less significant at higher DO range.

During the 2D tank experiment with ZVI applied, the strip of oxygen foil was analyzed using Matlab at 10min, 30min, 1hr and 2hr periods. The original RGB pictures were extracted to intensity figures, and a rectangle in the middle along the foil was selected to show vertical intensity profiles for later DO calculation purpose (Figure 4.6). At 10min, the aerated DI water only flowed through part of the mixture layer that left the bottom part lighter. The intensity maps at 30min, 1hr and 2hr periods were similar in colors that indicated a minimal time effect in this experiment. The intensity values along the vertical rectangle were then converted to DO values based on the calibration equations at respective time periods. The plots of DO values against vertical pixels at different time periods were shown in Figure 4.7. Gradients of DO at top half of the foil were observed that the values decreased at deeper depth, whereas the DO concentrations fluctuated at the bottom part. When time increased from 10min to 2hr, the DO profiles shifted from left to right toward higher DO values. Consistently with the intensity analysis, the DO profiles at 30min, 1hr and 2hr were similar, therefore the minimal time effect was observed at longer period.

4. Discussion

The performances of two optical sensor foils were evaluated through calibration tests and application experiments in simulated environments. Data (i.e. intensity)

extracted from images were used to reveal the temporal and spatial information with high resolutions.

4.1. pH foil performance in porous media

Calibration test of pH foil was conducted to relate the light intensity to pH values for later application experiment purpose. The intensity generally increased when pH value raised from 3 to 7. However, from pH of 6.5 to 7, the intensity did not show much difference, and a possible reason to explain this phenomenon was the self-absorption due to small Stokes shift. By definition, the Stokes shift represents the gap between the absorption and emission fluorescence spectra, and self-absorption is due to the overlap of the two. A wider Stokes shift is beneficial for easier fluorescence detection (Valeur and Berberan-Santos, 2012).

During application experiment, the extracted intensity map provided lots of information about the performance of the pH foil across the whole strip (Figure 4.3). The decrease in intensity color and value when time increased from 10min to 2hr was because less $CaCO_3$ was left to react with new acidic influent. The relative darker band on the top part became wider as time increased was also due to the fact that the continuing reaction between $CaCO_3$ and sulfuric acid influent. The winding flow marks formed at the bottom showed more obviously at longer period, and this might be the result of the flow bypassing pieces of $CaCO_3$. As shown in Figure 4.4, gradients of pH at top half of the foil were observed as the acidic flow continuing to react with mixed $CaCO_3$ and consume H^+ when moving downward. Consistently with the intensity map, when time increased, less $CaCO_3$ was left to react with influent and therefore the pH values reduced.

4.2. Oxygen foil performance in porous media

The phenomenon for oxygen foil calibration was opposite from the pH one, where higher DO concentration had a darker or less intense color. The reason for this was due to the quenching effect from oxygen, and the highest fluorescence intensity was observed when oxygen was absent (Rudolph et al., 2015). Study showed that temperature also had an effect on quenching behavior, in order to avoid unexpected error from temperature change, this research was conducted under the consistent room temperature (Baleizão et al., 2008). The calibration curve in the form of I_0/I gave a nonlinear plot, which was supported by the Stern-Volmer figure (Carraway et al., 1991b). The only difference was the direction of the curvature, where the curvature was upward in this test. Possible reason could be the case difference that data was completely empirical. The shifts among time periods shown in Figure 4.5 indicated that oxygen continuously reacted with foil in a relatively slower rate compared to pH foil one.

The intensity map from application experiment applied with ZVI showed less variation across the foil strip compared to the pH one (Figure 4.6). A clear decreasing gradient shown in Figure 4.7 indicated a continuous reaction between ZVI and oxygen along the depth. When time increased from 10min to longer periods, the DO concentration raised. This shift in DO was because of the consumption of ZVI, that less ZVI was available to react and consume oxygen when new influent flowed through. Minimal time effect reflected by the overlap of pH profiles at 30min, 1hr, and 2hr revealed a consistent reaction rate between ZVI and oxygen within this time period.

5. Conclusion

Evaluations of pH and oxygen foil in porous media were conducted through calibration tests in cuvettes and application experiments in 2D tank. Crushed $CaCO_3$ and ZVI were mixed with sand for pH and oxygen foils to react with, respectively. The results showed gradients of pH and DO concentration change along the vertical depth, where pH value increased and DO decreased. For pH foil, when time increased from 10min to 2hr, the pH continuously decreased and the pH profile shifted toward left. However, at time 30min, 1hr, and 2hr, oxygen foil did not show great difference in intensity and DO values among time periods, which was shown by the overlap of profiles. This might result from different reaction rates between applied materials and two sensor foils.

6. Figures

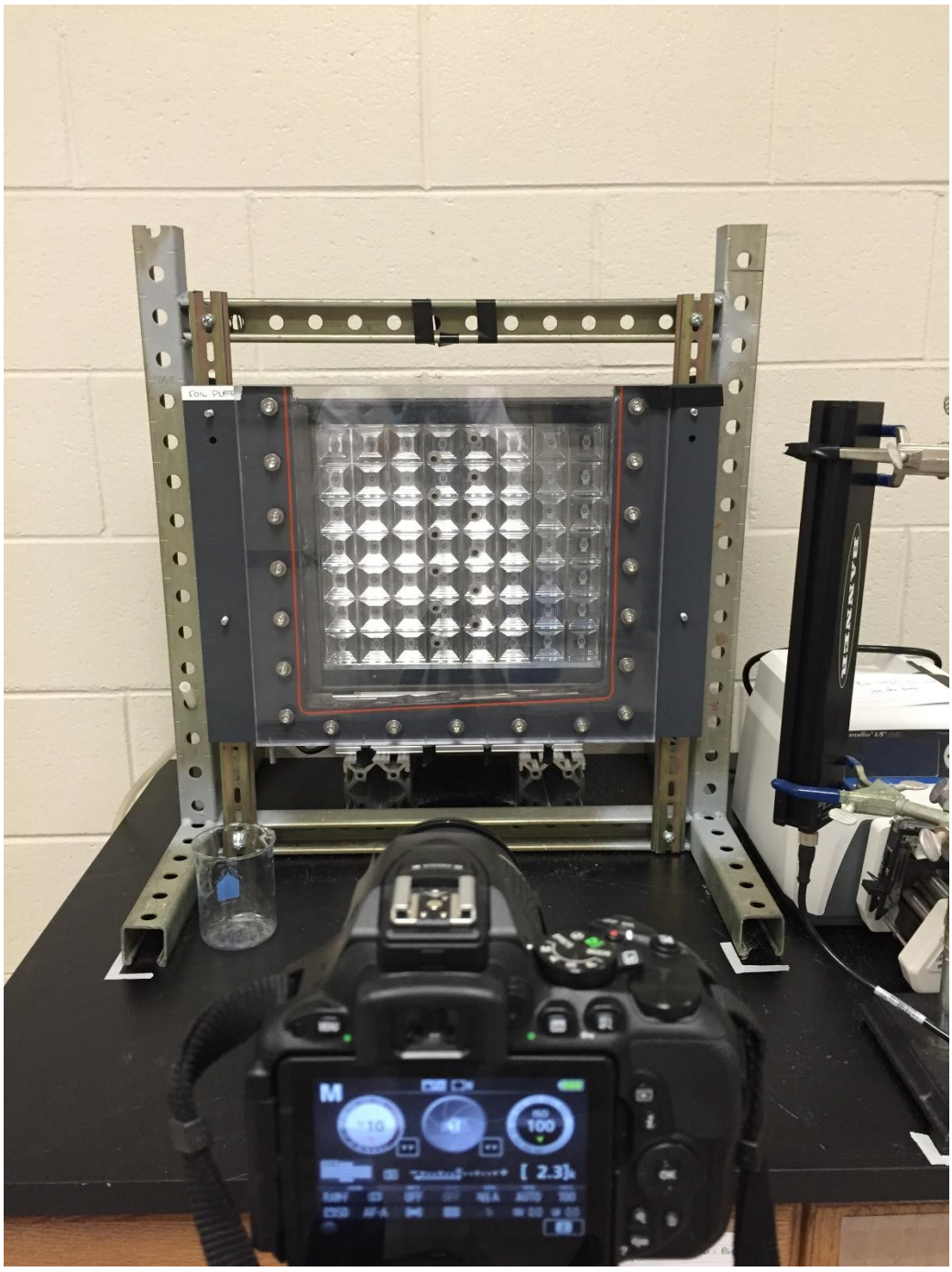

Figure 4.1 General setup of the experiment

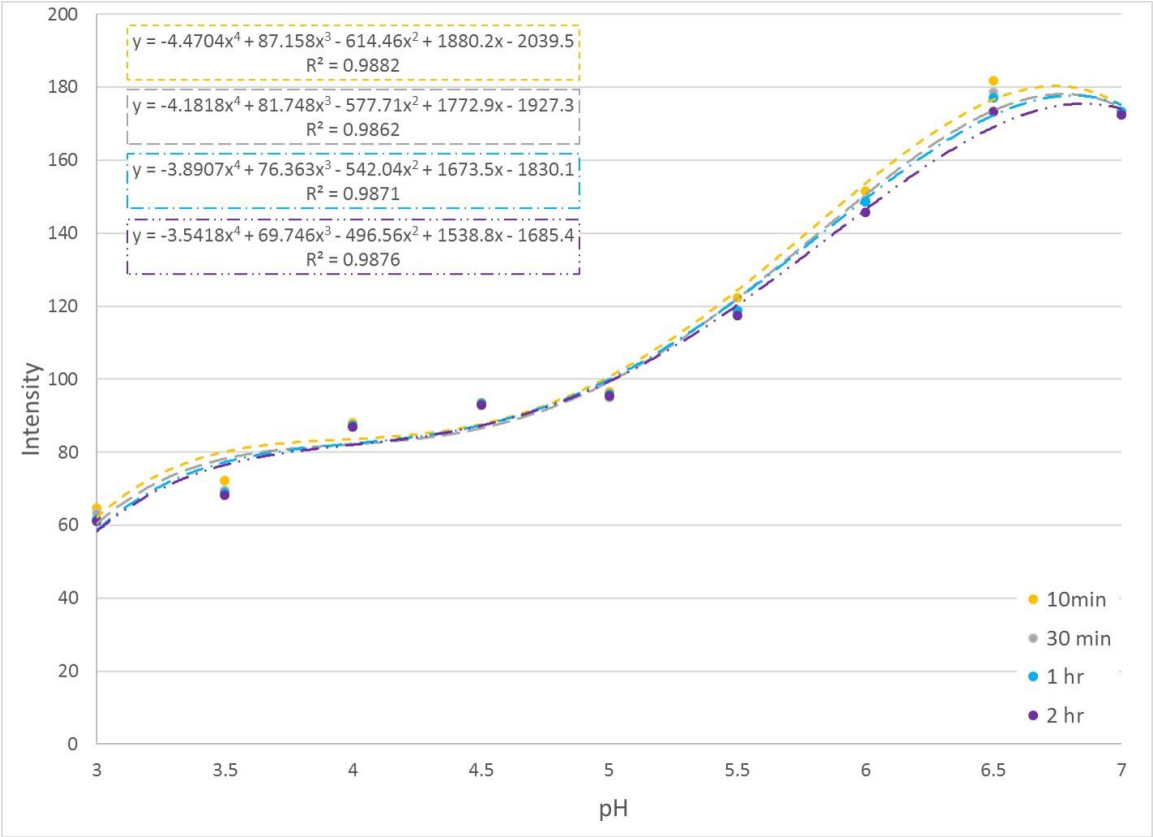

Figure 4.2 Calibration curve for pH sensor foil at time 10min, 30min, 1hr and 2hr

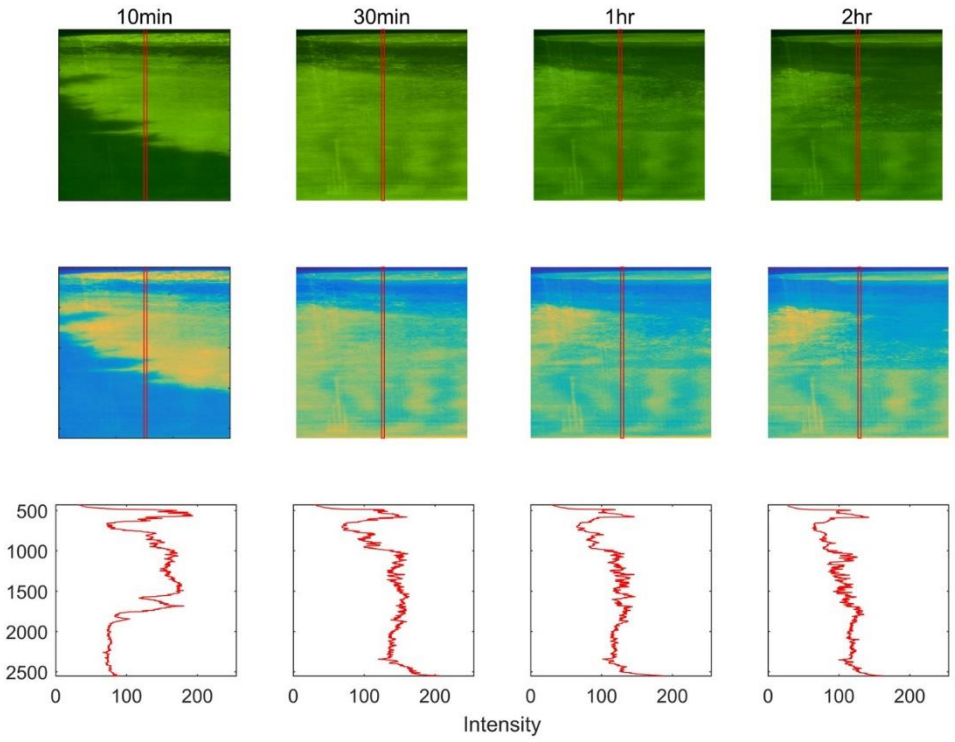

Figure 4.3 Processed image of application experiment for pH foil strip. First row: original RGB image; Second row: extracted intensity image; Third row: intensity profile based on the selected rectangle area

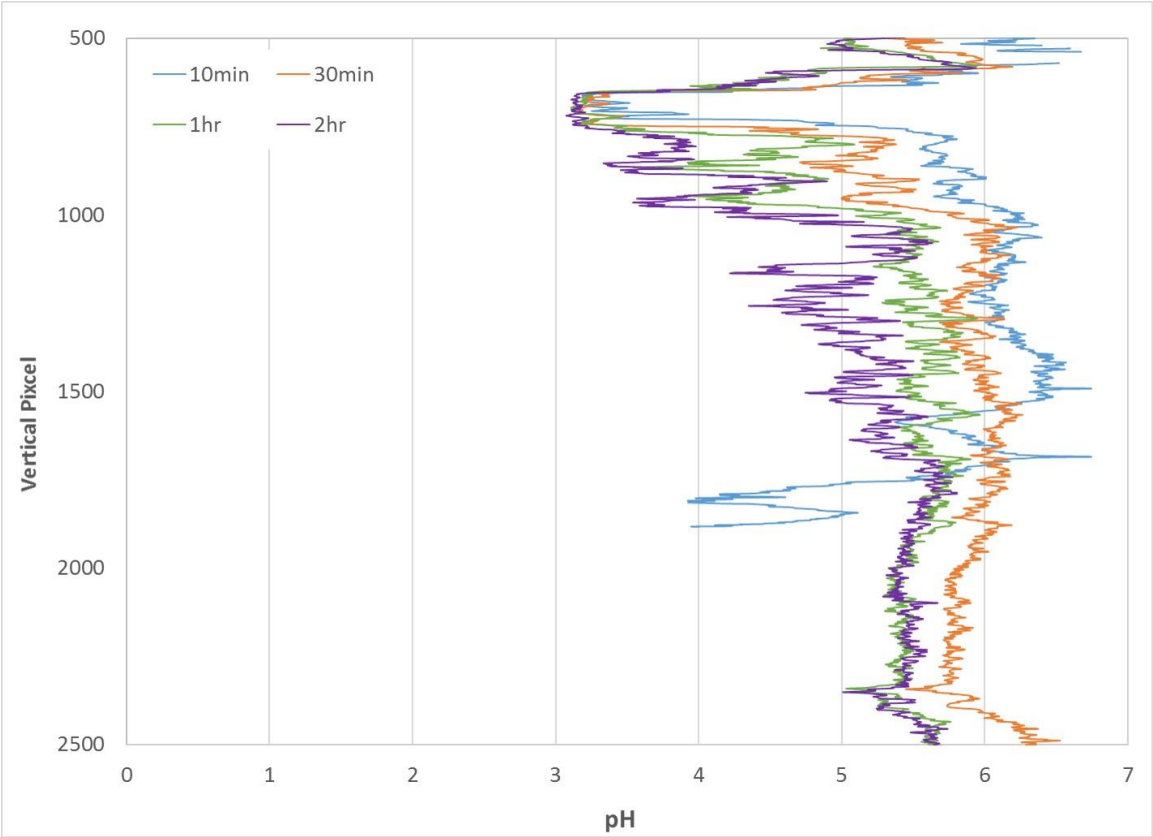

Figure 4.4 pH profile along vertical foil strip at time 10min, 30min, 1hr and 2hr

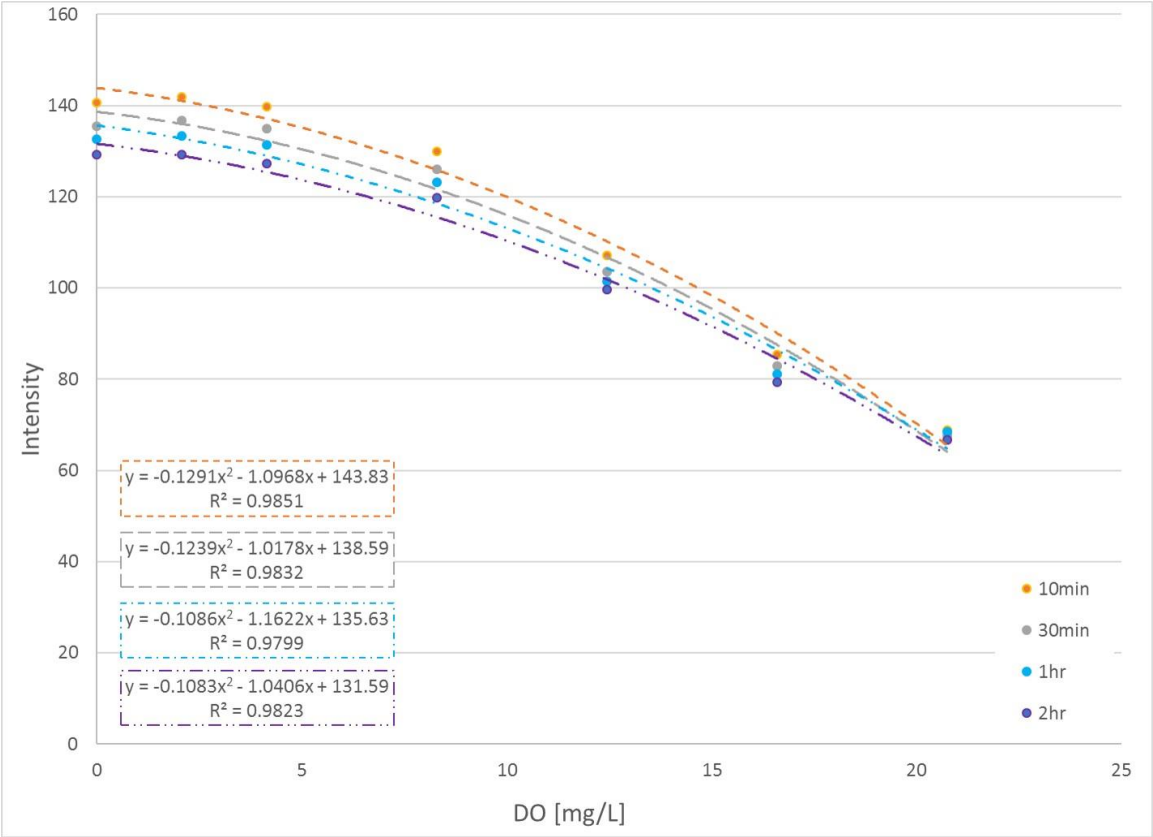

Figure 4.5 Calibration curve for oxygen sensor foil at time 10min, 30min, 1hr and 2hr

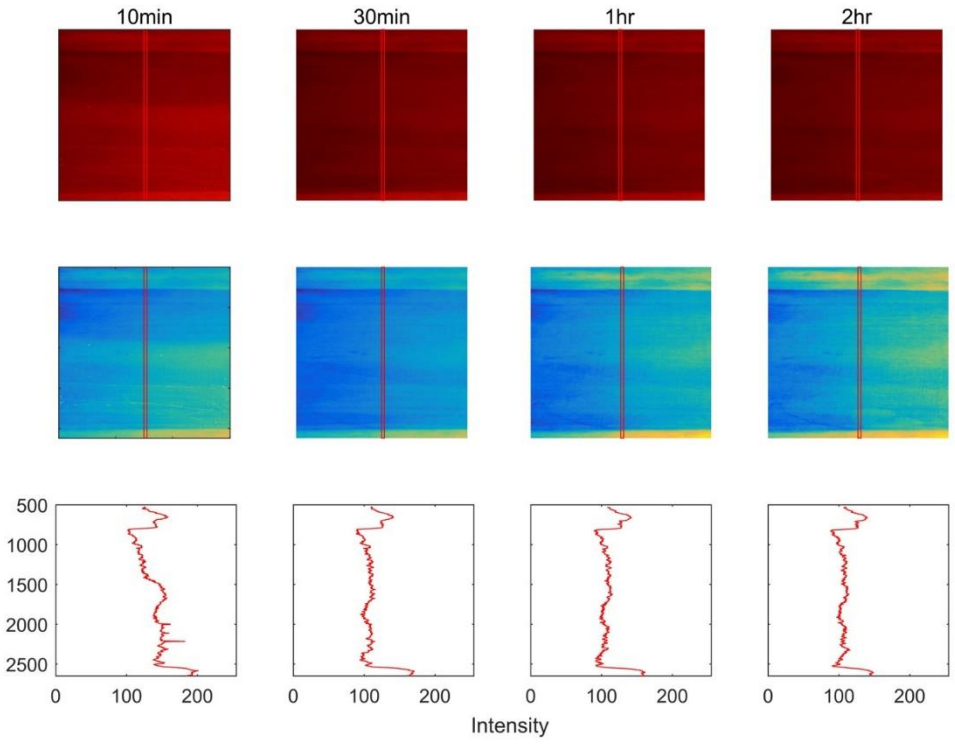

Figure 4.6 Processed image of application experiment for oxygen foil strip. First row: original RGB image; Second row: extracted intensity image; Third row: intensity profile based on the selected rectangle area

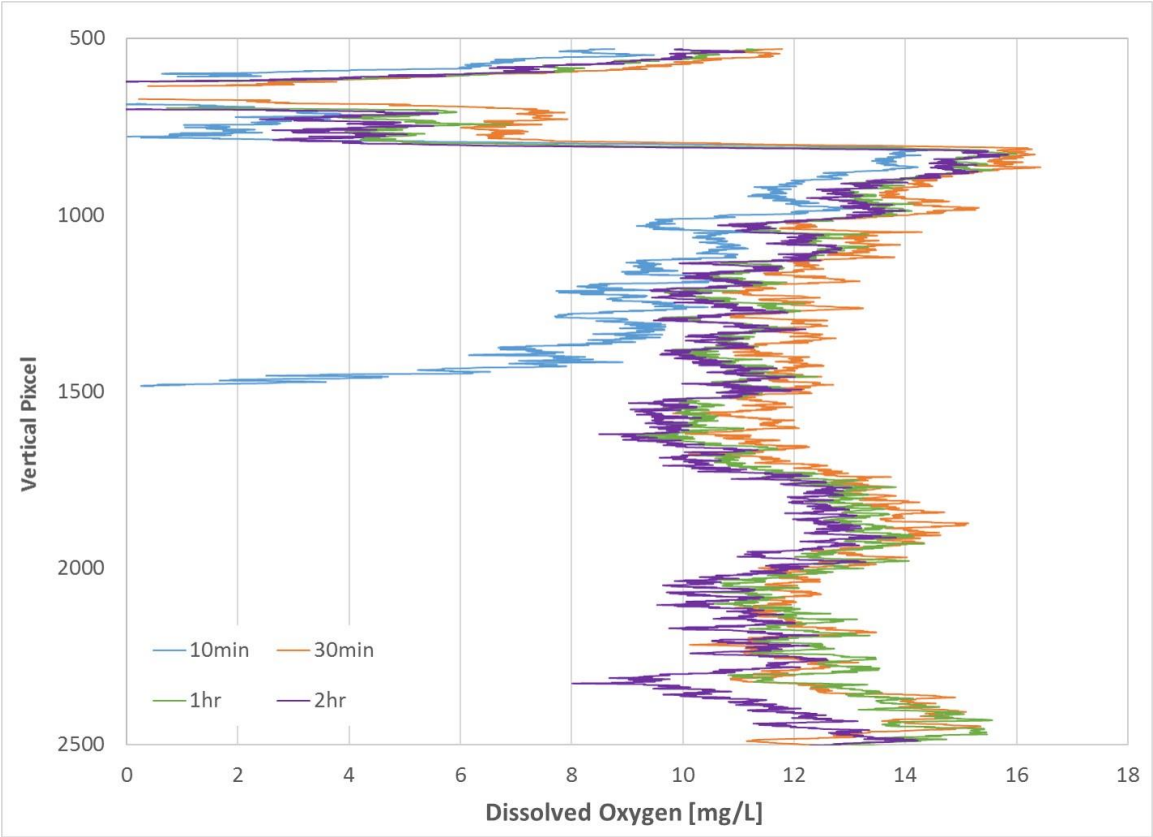

Figure 4.7 Dissolved oxygen concentration profile along vertical foil strip at time 10min, 30min, 1hr and 2hr

7. Acknowledgments

This material is based upon work supported by the U.S. Department of Energy Office of Science, Office of Basic Energy Sciences and Office of Biological and Environmental Research under Award Number DE-SC-00012530.

8. References

Akcil, A., Koldas, S., 2006. Acid Mine Drainage (AMD): causes, treatment and case studies. J. Clean. Prod. 14, 1139–1145. doi:10.1016/j.jclepro.2004.09.006

Baleizão, C., Nagl, S., Schäferling, M., Berberan-Santos, M.N., Wolfbeis, O.S., 2008. Dual Fluorescence Sensor for Trace Oxygen and Temperature with Unmatched Range and Sensitivity. Anal. Chem. 80, 6449–6457. doi:10.1021/ac801034p

Blossfeld, S., Gansert, D., 2007. A novel non-invasive optical method for quantitative visualization of pH dynamics in the rhizosphere of plants. Plant. Cell Environ. 30, 176–186. doi:10.1111/j.1365-3040.2006.01616.x

Blossfeld, S., Perriguey, J., Sterckeman, T., Morel, J.-L., Lösch, R., 2010. Rhizosphere pH dynamics in trace-metal-contaminated soils, monitored with planar pH optodes. Plant Soil 330, 173–184. doi:10.1007/s11104-009-0190-z

Borisov, S.M., Vasylevska, A.S., Krause, C., Wolfbeis, O.S., 2006. Composite Luminescent Material for Dual Sensing of Oxygen and Temperature. Adv. Funct. Mater. 16, 1536–1542. doi:10.1002/adfm.200500778

Brune, A., Frenzel, P., Cypionka, H., 2000. Life at the oxic–anoxic interface: microbial activities and adaptations. FEMS Microbiol. Rev. 24, 691–710. doi:10.1111/j.1574-

6976.2000.tb00567.x

Buekers, J., 2007. Fixation of cadmium, copper, nickel and zinc in soil: kinetics, mechanisms and its effect on metal bioavailability.

Calmano, W., Hong, J., Förstner, U., 1993. Binding and Mobilization of Heavy Metals in Contaminated Sediments Affected by pH and Redox Potential. Water Sci. Technol. 28, 223 LP-235.

Cameron, R.E., 1992. Guide to site and soil description for hazardous waste characterization [WWW Document]. Environ. Prot. Agency EPA.

Carraway, E.R., Demas, J.N., Degraff, B.A., 1991a. Luminescence Quenching Mechanism for Microheterogeneous Systems. Anal. Chem. 63, 332–336. doi:10.1021/ac00004a007

Carraway, E.R., Demas, J.N., DeGraff, B.A., Bacon, J.R., 1991b. Photophysics and photochemistry of oxygen sensors based on luminescent transition-metal complexes. Anal. Chem. 63, 337–342. doi:10.1021/ac00004a007

Christensen, T.H., 1984. Cadmium soil sorption at low concentrations: I. Effect of time, cadmium load, pH, and calcium. Water. Air. Soil Pollut. 21, 105–114. doi:10.1007/BF00163616

Chuan, M.C., Shu, G.Y., Liu, J.C., 1996. Solubility of heavy metals in a contaminated soil: Effects of redox potential and pH. Water. Air. Soil Pollut. 90, 543–556. doi:10.1007/BF00282668

Cundy, A.B., Hopkinson, L., Whitby, R.L.D., 2008. Use of iron-based technologies in contaminated land and groundwater remediation: A review. Sci. Total Environ. 400,

42–51. doi:10.1016/j.scitotenv.2008.07.002

Dube, A., Zbytniewski, R., Kowalkowski, T., Cukrowska, E., Buszewski, B., 2001. Adsorption and Migration of Heavy Metals in Soil. Polish J. Environ. Stud. 10, 1–10.

Fischer, W.R., Flessa, H., Schaller, G., 1989. pH values and redox potentials in microsites of the rhizosphere. Zeitschrift für Pflanzenernährung und Bodenkd. 152, 191–195. doi:10.1002/jpln.19891520209

Fu, F., Dionysiou, D.D., Liu, H., 2014. The use of zero-valent iron for groundwater remediation and wastewater treatment: A review. J. Hazard. Mater. 267, 194–205. doi:10.1016/j.jhazmat.2013.12.062

Fuller, Z.J., Bare, W.D., Kneas, K.A., Xu, W.-Y., Demas, J.N., DeGraff, B.A., 2003. Photostability of Luminescent Ruthenium(II) Complexes in Polymers and in Solution. Anal. Chem. 75, 2670–2677. doi:10.1021/ac0261707

Glud, R.N., Ramsing, N.B., Gundersen, J.K., Klimant, I., 1996. Planar optrodes: a new tool for fine scale measurements of two-dimensional O 2 distribution in benthic communities. Mar. Ecol. Prog. Ser. 140, 217–226.

Glud, R.N., Santegoeds, C.M., De Beer, D., Kohls, O., Ramsing, N.B., 1998. Oxygen dynamics at the base of a biofilm studied with planar optodes. Aquat. Microb. Ecol. 14, 223–233. doi:10.3354/ame014223

Gregory, P.J., Hinsinger, P., 1999. New approaches to studying chemical and physical changes in the rhizosphere: an overview. Plant Soil 211, 1–9. doi:10.1023/A:1004547401951

Hinsinger, P., Bengough, A.G., Vetterlein, D., Young, I.M., 2009. Rhizosphere: biophysics, biogeochemistry and ecological relevance. Plant Soil 321, 117–152. doi:10.1007/s11104-008-9885-9

Hinsinger, P., Gobran, G.R., Gregory, P.J., Wenzel, W.W., 2005. Rhizosphere geometry and heterogeneity arising from root-mediated physical and chemical processes. New Phytol. 168, 293–303. doi:10.1111/j.1469-8137.2005.01512.x

Huang, W.E., Oswald, S.E., Lerner, D.N., Smith, C.C., Zheng, C., 2003. Dissolved Oxygen Imaging in a Porous Medium to Investigate Biodegradation in a Plume with Limited Electron Acceptor Supply. Environ. Sci. Technol. 37, 1905–1911. doi:10.1021/es020128b

Jaillard, B., Ruiz, L., Arvieu, J.-C., 1996. pH mapping in transparent gel using color indicator videodensitometry. Plant Soil 183, 85–95. doi:10.1007/BF02185568

Johnson, D.B., Hallberg, K.B., 2005. Acid mine drainage remediation options: a review. Sci. Total Environ. 338, 3–14. doi:10.1016/j.scitotenv.2004.09.002

Kanungo, S.B., Mohapatra, R., 2000. Leaching behavior of various trace metals in aqueous medium from two fly ash samples. J. Environ. Qual. 29, 188–196.

Kleinmann, R.L.P., Hedin, R.S., Nairn, R.W., 1998. Treatment of Mine Drainage by Anoxic Limestone Drains and Constructed Wetlands, in: Geller, W., Klapper, H., Salomons, W. (Eds.), Acidic Mining Lakes: Acid Mine Drainage, Limnology and Reclamation. Springer Berlin Heidelberg, Berlin, Heidelberg, pp. 303–319. doi:10.1007/978-3-642-71954-7_16

Klimant, I., Meyer, V., Kühl, M., 1995. Fiber-optic oxygen microsensors, a new tool in

aquatic biology. Limnol. Oceanogr. 40, 1159–1165. doi:10.4319/lo.1995.40.6.1159

Kot, A., Namieśnik, J., 2000. The role of speciation in analytical chemistry. TrAC Trends Anal. Chem. 19, 69–79. doi:10.1016/S0165-9936(99)00195-8

Levy, D.B., Barbarick, K.A., Siemer, E.G., Sommers, L.E., 1992. Distribution and partitioning of trace metals in contaminated soils near Leadville, Colorado. J. Environ. Qual. 21, 185–195.

Liebsch, G., Klimant, I., Frank, B., Holst, G., Wolfbeis, O.S., 2000. Luminescence Lifetime Imaging of Oxygen, pH, and Carbon Dioxide Distribution Using Optical Sensors. Appl. Spectrosc. 54, 548–559. doi:10.1366/0003702001949726

McEvoy, A.K., McDonagh, C.M., MacCraith, B.D., 1996. Dissolved Oxygen Sensor Based on Fluorescence Quenching of Oxugen-Sensitive Ruthenium Complexes Immobilized in Sol-Gel-derived Porous Silica Coatings. Analyst 121, 785–788.

Morrison, S.J., Metzler, D.R., Dwyer, B.P., 2002. Removal of As, Mn, Mo, Se, U, V and Zn from groundwater by zero-valent iron in a passive treatment cell: reaction progress modeling. J. Contam. Hydrol. 56, 99–116. doi:10.1016/S0169-7722(01)00205-4

Mulligan, C.N., Yong, R.N., Gibbs, B.F., 2001. Remediation technologies for metal-contaminated soils and groundwater: an evaluation. Eng. Geol. 60, 193–207. doi:10.1016/S0013-7952(00)00101-0

Precht, E., Franke, U., Polerecky, L., Huettel, M., 2004. Oxygen dynamics in permeable sediments with wave-driven pore water exchange. Limnol. Oceanogr. 49, 693–705. doi:10.4319/lo.2004.49.3.0693

Rangsivek, R., Jekel, M.R., 2005. Removal of dissolved metals by zero-valent iron (ZVI): Kinetics, equilibria, processes and implications for stormwater runoff treatment. Water Res. 39, 4153–4163. doi:10.1016/j.watres.2005.07.040

Rudolph, N., Esser, H.G., Carminati, A., Moradi, A.B., Hilger, A., Kardjilov, N., Nagl, S., Oswald, S.E., 2012. Dynamic oxygen mapping in the root zone by fluorescence dye imaging combined with neutron radiography. J. Soils Sediments 12, 63–74. doi:10.1007/s11368-011-0407-7

Rudolph, N., Gottfried, S., Lamshöft, M., Zühlke, S., Oswald, S.E., Spiteller, M., 2015. Non-invasive imaging techniques to study O2 micro-patterns around pesticide treated lupine roots. Geoderma 239–240, 257–264. doi:10.1016/j.geoderma.2014.10.022

Schaller, G., Fischer, W.R., 1985. pH-Änderungen in der Rhizosphäre von Mais- und Erdnußwurzeln. Zeitschrift für Pflanzenernährung und Bodenkd. 148, 306–320. doi:10.1002/jpln.19851480310

Scherer, M.M., Richter, S., Valentine, R.L., Alvarez, P.J.J., 2000. Chemistry and Microbiology of Permeable Reactive Barriers for In Situ Groundwater Clean up. Crit. Rev. Microbiol. 26, 221–264. doi:10.1080/10408410091154237

Schröder, C.R., Polerecky, L., Klimant, I., 2007. Time-resolved pH/pO2 mapping with luminescent hybrid sensors. Anal. Chem. 79, 60–70. doi:10.1021/ac0606047

Sun, L., Chen, S., Chao, L., Sun, T., 2007. Effects of Flooding on Changes in Eh, pH and Speciation of Cadmium and Lead in Contaminated Soil. Bull. Environ. Contam. Toxicol. 79, 514–518. doi:10.1007/s00128-007-9274-8

Valeur, B., Berberan-Santos, M.N., 2012. Molecular fluorescence: principles and applications, Second. ed. John Wiley & Sons.

Violante, A., Cozzolino, V., Perelomov, L., Caporale, A.G., Pigna, M., 2010. Mobility and bioavailability of heavy metals and metalloids in soil environments. J. soil Sci. plant Nutr. 10, 268–292. doi:10.4067/S0718-95162010000100005

Weidgans, B.M., Krause, C., Klimant, I., Wolfbeis, O.S., 2004. Fluorescent pH sensors with negligible sensitivity to ionic strength. Analyst 129, 645–650. doi:10.1039/b404098h

Weisenseel, M.H., Dorn, A., Jaffe, L.F., 1979. Natural H+ currents traverse growing roots and root hairs of barley (Hordeum vulgare L.). Plant Physiol. 64, 512–518.

Werth, C.J., Zhang, C., Brusseau, M.L., Oostrom, M., Baumann, T., 2010. A review of non-invasive imaging methods and applications in contaminant hydrogeology research. J. Contam. Hydrol. 113, 1–24. doi:10.1016/j.jconhyd.2010.01.001

Wuana, R.A., Okieimen, F.E., 2011. Heavy Metals in Contaminated Soils: A Review of Sources, Chemistry, Risks and Best Available Strategies for Remediation. ISRN Ecol. 2011. doi:10.5402/2011/402647

CHAPTER FIVE

CONCLUSION

The first study evaluated the enzyme activity with CeO_2 nanoparticles applied in porous soil media. Higher NP concentration above and equal to 100 mg/kg was found to inhibit the urease and ß-glucosidase activities, and to stimulate the phosphatase activity. Specifically, the inhibition effect from CeO_2 NPs on urease activity for the non-cut 1 and cut 1 groups increased from a -5.07% at a 100 mg/kg concentration to -13.2% at a 500 mg/kg concentration to -19.91% at a 1000 mg/kg concentration compared to the treatment without CeO_2 NPs. The inhibition effect from CeO_2 NPs on beta glucosidase activity for the cut 2 group, increased from -0.32% to -70.84% at the 100 mg/kg and 1000 mg/kg concentrations, while an inhibition percentage for the non-cut 2 group was between -16.89% to -50.22% at the 100 mg/kg and 1000 mg/kg concentrations. The non-cut and cut 1 groups exhibited the greatest effect on promotion of the phosphatase activity, with an increase from 97.46% to 131.37% to 181.45% at 100, 500 and 1000 mg/kg concentrations, respectively, compared to the 0 mg/kg concentration. The aging effect of CeO_2 NPs indicated that a longer contact time between NPs and the soil alleviated the impact from CeO_2 NPs on soil enzymes, and potentially reduced the ecotoxicity of NPs in soil environment.

The second study investigated the preferential flow in two-dimensional (2D) sand system with microbial exudates applied. The experimental results showed that the microbial exudate addition affected the infiltration process by differing from the control NaCl solution, which was possibly due to an improved water holding capacity. Moreover,

a higher wettability was observed in the catechol solution at an increased concentration. Although the wettability of the medium for riboflavin solution decreased with an increase in concentration, very little change was observed for the other flow characteristics. These results of water profile analysis and comparison of the interfacial parameters, in addition to the water holding capacity, are expected to elucidate the microbial exudates interacting with preferential flow pattern, and also reveal the importance of the infiltration process on microbial activity.

The third study measured the pH and dissolved oxygen concentration in 2D sand system using optical sensor technique. Application tests of sensor foils involved zero valent iron (ZVI) and sulfuric acid drainage solution in order to obtain gradients of parameter changes. Results showed that gradients were formed at the top half of the foil. Based on the data obtained at time 10min, 30min, 1hr, and 2hr, the time effect on pH foil was greater than that on the oxygen foil.

Although the three studies were independent researches, they could be related in the aspects of contaminant evaluation and various approaches of measuring biological and physiochemical parameters in porous media systems.

APPENDIX

Appendix A

Supplementary Figure for Chapter Four

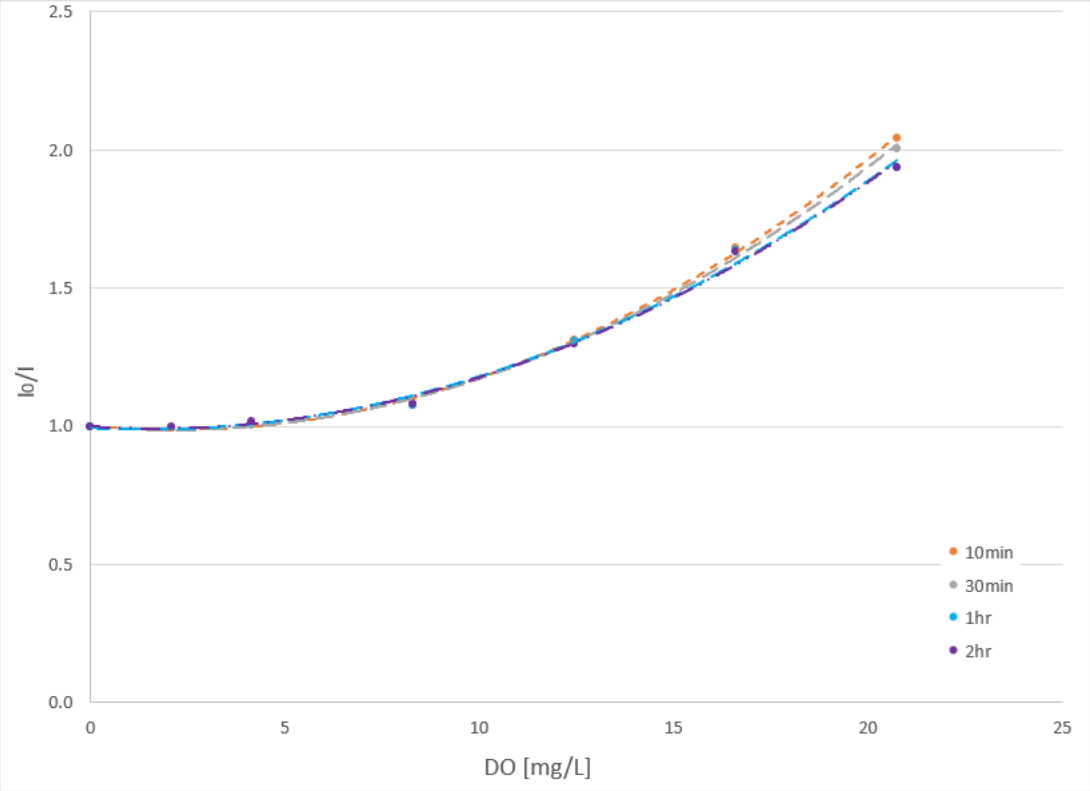

Figure A-1: Oxygen foil calibration curve in the form of I_0/I against dissolved oxygen concentration among time periods.